Chemical Engineering Research and Design 230 (2026) 698–717

Contents lists available at ScienceDirect

Chemical Engineering Research and Design

journal homepage: www.elsevier.com/locate/cherd

Self-optimizing control of fully electrified heat pump assisted distillation process by flash vapor circulation

Chengtian Cui [a,b,*], Xiaodong Zhang [c], Meng Qi [d], Sigurd Skogestad [e], Anton A. Kiss [b,**]

[a] Process and Systems Engineering Laboratory, Åbo Akademi University, Turku 20500, Finland
[b] Department of Chemical Engineering, Delft University of Technology, Delft 2629 HZ, the Netherlands
[c] College of Smart Energy, Shanghai Jiao Tong University, Shanghai 200240, China
[d] Department of Chemistry and Bioscience, Aalborg University, Esbjerg 6700, Denmark
[e] Department of Chemical Engineering, Norwegian University of Science and Technology (NTNU), Trondheim 7491, Norway

A R T I C L E I N F O

Keywords:
Self-optimizing control
Process electrification
Heat pump assisted distillation
Flash vapor circulation

A B S T R A C T

A fully electrified flash vapor circulation (FVC) distillation system for methanol/water separation is investigated, with a focus on identifying suitable self-optimizing controlled variables for minimizing electric power consumption. Starting from two published schemes (CS1 and CS2), four new control structures (CS3 – CS6) are developed to explain and remove the strongly asymmetric closed-loop behavior observed in the original designs. Closed-loop dynamic simulations are performed under ± 20% step disturbances in throughput and methanol composition. Control performance is assessed using product quality deviations, energy indicators, settling time, and integrated absolute error. The results show that controlling compressor discharge pressure in CS1 and CS2 is a poor choice because it over-constrains the series pressure loop of the FVC configuration, which drives excessive recycle, asymmetric responses, and COP deterioration. Eliminating this redundant pressure constraint in CS3 restores the available degrees of freedom and yields more symmetric behavior with lower compression power. Building on self-optimizing control, CS4 and CS5 select condenser outlet conditions as controlled variables to coordinate the trade-off between pressure lift and circulating vapor flow, giving similar energy performance. Finally, CS6 adds a distillate composition controller on top of CS4 to enforce the methanol specification and avoid both under and over purification, with only longer transients due to the slower composition loop. To generalize these findings, a three-step workflow is proposed as a transferable design procedure for heat pump assisted distillation systems.

1. Introduction

Electrification of the chemical industry has attracted increasing attention in recent years, as low-carbon electricity from wind and solar power is expected to become more abundant (Kiss and Smith, 2020; Qi et al., 2025). An important component of electrified process technology is the use of heat pumps in process units, where electrically driven compressors are employed to supply larger amounts of thermal energy. Mechanical vapor recompression (MVR) applied to distillation columns has therefore been widely studied (Adami et al., 2025a, 2025b; Cui et al., 2025b, 2024a; Cui and Kiss, 2026; Kiss and Infante Ferreira, 2016). From a control perspective, however, when a heat pump is integrated, the condenser and reboiler duties become coupled rather than independent (Cui et al., 2025a, 2022; Jogwar and Daoutidis, 2009; Karami et al., 2015; Patraşcu et al., 2019, 2017; Yang et al., 2025b, 2023). Compared to a conventional distillation column with independent condenser and reboiler, an MVR-assisted column thus loses one control degree of freedom (CDOF). A common way to recover this lost CDOF is to add a trim reboiler and/or a trim condenser. This generally simplifies control and reduces the load on the compressor, which can also be beneficial in terms of capital cost (Luyben, 2026, 2018).

For a distillation column with a subcooled liquid feed, one would typically expect the reboiler duty to be larger than the condenser duty, so that ideally only a trim reboiler is needed when using MVR (Fig. 1**a**). This trim reboiler duty can alternatively be supplied through feed preheating (Fig. 1**b**) (Yang et al., 2025a). However, the trim reboiler and/or

* Corresponding author at: Process and Systems Engineering Laboratory, Åbo Akademi University, Turku 20500, Finland.
** Corresponding author.
E-mail addresses: Chengtian.Cui@abo.fi (C. Cui), A.A.Kiss@tudelft.nl (A.A. Kiss).

https://doi.org/10.1016/j.cherd.2026.05.017
Received 1 February 2026; Received in revised form 3 May 2026; Accepted 9 May 2026
Available online 13 May 2026

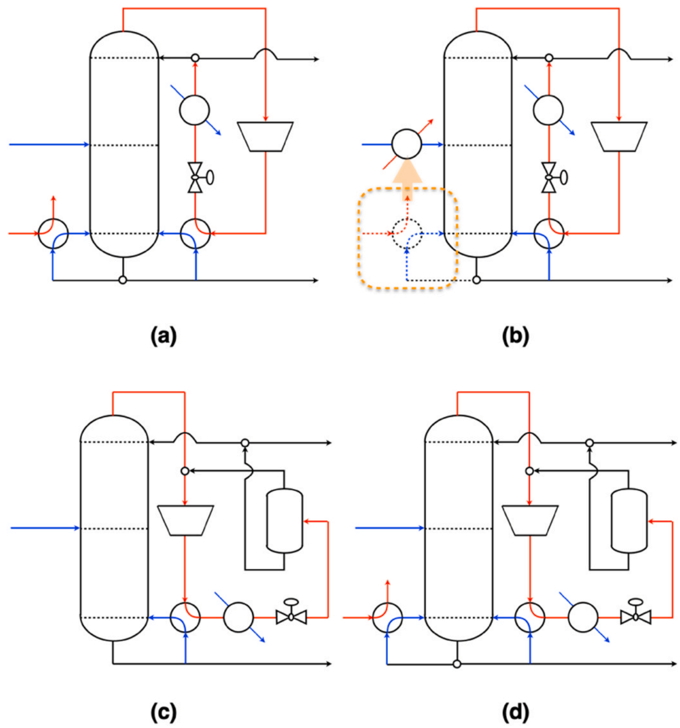

Fig. 1. (a) MVR with trim reboiler; (b) MVR with feed preheating; (c) Proposed FVC; (d) FVC with trim reboiler.

feed preheater can be eliminated by using our recently proposed flash vapor circulation (FVC) configuration (Fig. 1**c**) (Cui et al., 2024b). The main idea of FVC is to remove the auxiliary heat exchangers (trim reboiler and/or feed preheater) by circulating more vapor in the heat pump loop, thereby increasing the amount of upcycled heat available to drive the distillation column. In other words, FVC attempts to use compressor power as an effective "trim reboiler". This is advantageous because the coefficient of performance (COP) of FVC is higher than that obtained when using electric heaters or electrode boilers to supply the column duty. The COP is defined as the ratio of useful heat delivered to the column to the electric power input to the compressors:

$$COP = \frac{Q_{reb}}{W_{comp}} \tag{1}$$

It is also interesting to note that the FVC process has a trim condenser. As we will prove in the next section, the trim condenser duty should be minimized to achieve optimal operation. In addition, it should be noted that FVC does not necessarily eliminate the trim reboiler under all operating conditions. In practice, the industrial deployment of fully electrified heat pump assisted distillation introduces critical operability challenges related to electrification constraints, such as variable electricity availability, dynamic pricing, and strict compressor capacity limits. To adapt to these varying loads, the use of variable-speed compressors has been actively investigated to manipulate the heat pump capacity and maintain control over the distillation column under changing operating conditions (Khan et al., 2012). However, variable-speed compressors are ultimately subject to mechanical and aerodynamic constraints, including maximum rotational speed, power bounds, and allowable pressure ratios. Karami et al. (2015) previously highlighted that effectively integrating heat pumps into distillation systems requires careful controllability analysis to avoid bottlenecks when such operational constraints are reached. To bridge this gap and ensure robust continuous operation, explicit constraint management strategies such as active constraint switching and split-range control are essential (Reyes-Lúa, 2020). For instance, Patraşcu et al. (2017) demonstrated that adding an auxiliary external duty stream with a bypass can effectively stabilize heat pump assisted distillation columns under thermal unbalance and operational constraints. In similar advanced constraint-handling designs, a small trim reboiler (Fig. 1**d**) can be operated via a split-range controller as a backup to the heat pump (Skogestad, 2023). The variable-speed compressor remains the primary actuator to supply base-load reboiler duty; if the compressor saturates due to grid constraints or speed limits, the split-range logic automatically brings the trim reboiler online to cover the remaining heat deficit. The present study focuses on low-loss self-optimizing operation of the FVC system in an unconstrained operating regime, where compressor saturation and grid-following power limits are not explicitly activated. Integrating split-range constraint-handling designs with a backup trim reboiler remains an important future extension for highly flexible electrified plants.

To investigate the control performance of the proposed FVC process in Fig. 1c, we recently proposed two control structures CS1 and CS2 for a methanol (MeOH)/water distillation case study (Cui et al., 2025c). CS1 utilizes single-end temperature control (TC) with a fixed compressor pressure and a fixed reflux ratio to handle ± 20% step changes in throughput and feed composition. The results show that CS1 provides generally satisfactory control; however, for a − 20% composition disturbance, the deviation in the target MeOH purity becomes non-negligible. To correct this, CS2 introduces composition control (CC) to directly regulate the target methanol product purity by manipulating the reflux ratio (RR). Overall, CS1 and CS2 demonstrate that an FVC-assisted distillation process can be operated in closed-loop, but they also bring significant energy penalty in terms of compressor power. In addition, markedly asymmetric dynamic responses are observed under certain disturbances. For example, in CS1, a + 20% throughput disturbance drives the FVC flow rate to approximately 6 times its nominal value and decreases the COP from its nominal value of 4.70–3.79. In contrast, when a − 20% throughput disturbance is introduced, the FVC flow rate decreases to 0.47 times the nominal value, while the COP increases to 4.83.

To diagnose the origin of the asymmetric behaviors and mitigate the resulting limitations on energy-efficient operation, this work develops new control strategies based on the concept of self-optimizing control (SOC). SOC is when an acceptable (economic) loss can be achieved using constant setpoints for the controlled variables (CVs), without the need to reoptimize when disturbances occur (Jäschke et al., 2017; Larsson et al., 2001; Skogestad, 2000; Zhang et al., 2024, 2023). In CS1 and CS2, the compressor discharge pressure is kept at a constant setpoint. However, as shown in this paper, this is a poor self-optimizing CV. Therefore, building on this concept, suitable self-optimizing CVs are identified and the associated control structures are evaluated under large disturbances. Overall, this work provides a systematic route to (near-)optimal operation while restoring symmetric dynamic responses.

This paper is organized as follows. Section 2 identifies the key factors for energy-efficient operation of the FVC heat pump loop. Section 3 presents a degrees of freedom analysis and uses it to explain the asymmetric behavior of CS1 and CS2. Section 4 develops the intermediate control structure CS3 by removing the redundant compressor discharge pressure constraint. Section 5 then focuses on selecting condenser outlet conditions as self-optimizing CVs and evaluating the resulting structures CS4 and CS5, followed by CS6 where a CC is added to enforce the MeOH specification. Section 6 compares all structures using dynamic performance and energy metrics. Section 7 concludes the main findings and implications.

2. Connection between compressor power and trim condenser duty

The present paper is the third contribution in a series on the same FVC distillation system. The underlying steady-state process basis, including the basic FVC configuration and thermodynamics, follows our earlier study (Cui et al., 2024b), while the base dynamic model and the previously reported control structures CS1 and CS2 follow our subsequent control paper (Cui et al., 2025c). Unless otherwise stated, these previously established model elements are retained in the present work.

To clarify the role of the trim condenser in the fully electrified FVC system in Fig. 1**c**, we consider an overall steady-state energy balance of the process (Fig. 2). The envelope encloses the heat pump loop associated with FVC. The column overhead vapor enters this envelope with vapor flow rate V_t and enthalpy flow H_{in}. Inside the envelope, the vapor is compressed in three stages with shaft works W_1, W_2, and W_3 (total compression power is $W_{comp} = W_1 + W_2 + W_3$). The compressed vapor is then condensed while delivering useful heat labelled Q_1, Q_2, and Q_3 to the column through the three heat exchangers. Herein, heat added to the envelope is defined as positive and heat removed from the envelope is defined by its magnitude. Surplus heat that cannot be utilized by the column is finally rejected to the trim condenser (Q_{trim}). The condensed liquid leaves the envelope with liquid flow rate L_t ($L_t = V_t$) and enthalpy flow H_{out}. The boilup vapor flow rate is V_b, with the corresponding reboiler duty given by Q_{reb}.

At steady-state, an overall energy balance around the envelope gives:

$$H_{in} + W_{comp} = H_{out} + (Q_1 + Q_2 + Q_3) + Q_{trim} \tag{2}$$

For the overhead stream at the column pressure, the enthalpy difference between incoming saturated vapor and outgoing liquid can be expressed by the latent heat of condensation, which also equals the condenser duty of a conventional column without heat pump (Q_{cond}):

$$Q_{cond} = H_{in} - H_{out} = V_t \bullet \Delta h_{vap,t} \tag{3}$$

The reboiler duty can be expressed as the product of column boilup rate and the latent heat of vaporization:

$$Q_{reb} = Q_1 + Q_2 + Q_3 = V_b \bullet \Delta h_{vap,b} \tag{4}$$

Substituting Eqs. (3–4) into (2) yields:

$$W_{comp} = Q_{trim} + (V_b \bullet \Delta h_{vap,b} - V_t \bullet \Delta h_{vap,t}) \tag{5}$$

For convenience, we define the term in parentheses as:

$$\Phi = V_b \bullet \Delta h_{vap,b} - V_t \bullet \Delta h_{vap,t} = Q_{reb} - Q_{cond} \tag{6}$$

So that Eq. (5) can be rewritten compactly as:

$$W_{comp} = Q_{trim} + \Phi \tag{7}$$

The important point about Eq. (7) is the close connection between the compression power W_{comp} and the trim condenser duty Q_{trim}. For a conventional column without heat pump, the quantity Φ represents the difference between the reboiler duty Q_{reb} and the condenser duty Q_{cond}. For columns with a saturated liquid feed, Φ is often close to zero, which is closely related to the constant molar overflow assumption in distillation (Cui et al., 2018). For a subcooled liquid feed, it is likely to have $\Phi > 0$. In this study, an equimolar MeOH/water (0.5/0.5) feed enters at 30 °C, which is subcooled. Table 1 summarizes the resulting values of Φ with the distillate MeOH purity specified at 0.99 and the bottoms water purity at 0.9999.

This work uses compressor power as the main economic objective for optimal operation:

$$J = W_{comp} \tag{8}$$

Eq. (7) shows that reducing Q_{trim} directly reduces W_{comp} for a given value of Φ. Therefore, identifying self-optimizing CVs that reliably reflect or constrain Q_{trim} is a practical way to achieve optimal operation (or low-loss self-optimizing operation).

In previous steady-state analysis (Cui et al., 2024b), we identified a minimum trim condenser duty threshold of approximately 183 kW (by setting the condenser outlet stream degree of subcooling as 39 °C). In the present work, this limit is revised to 185 kW to account for the inclusion of the circulation pump. Below this threshold, a temperature crossover occurs in the reboiler, given the minimum allowable temperature approach of 10 °C.

3. Analysis of the existing control structures CS1 and CS2

The main issues with the existing CS1 and CS2 are strong asymmetric responses and high compressor power consumption (Cui et al., 2025c). To identify the source of the asymmetry and to improve low-loss operation, the existing schemes are re-examined. CS2 differs from CS1 only by the inclusion of an additional CC, while all other control loops remain identical. Consequently, both structures exhibit essentially the same

Table 1
Values of Φ under various disturbances.

	Nominal	+ 20% F	− 20% F	+ 20% MeOH	− 20% MeOH
Φ (kW)	118.4	143.6	93.8	100.0	133.9

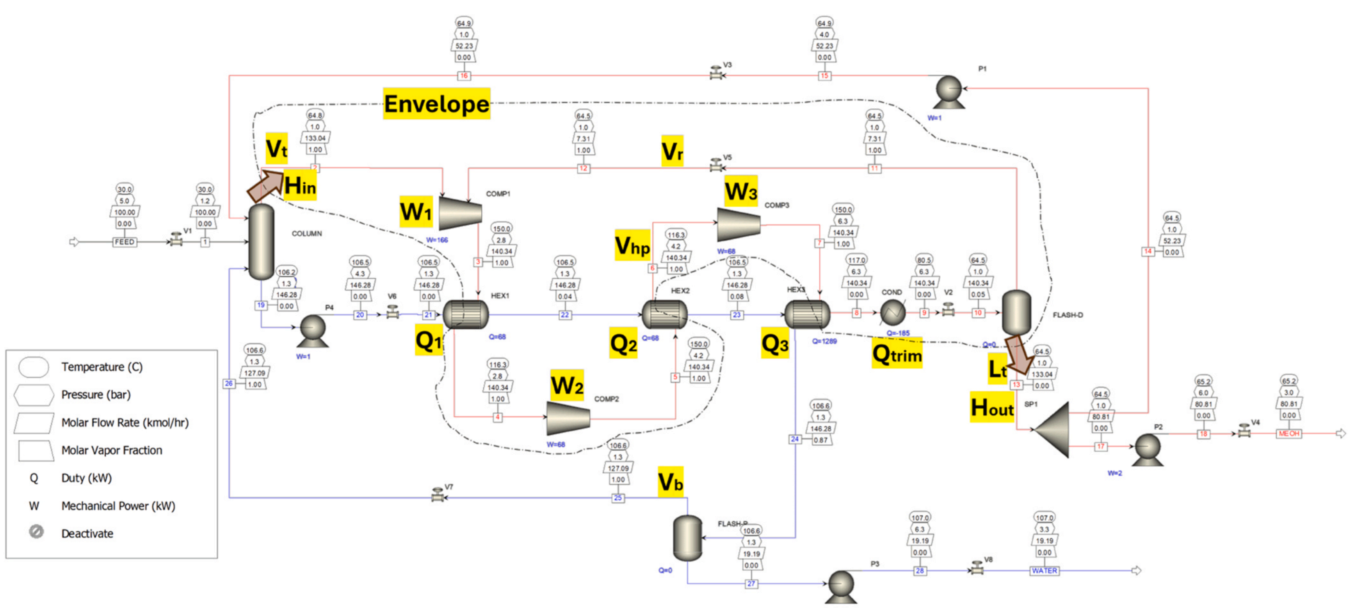

Fig. 2. Steady-state flowsheet.

control limitations. Fig. 3 shows CS1 together with its Aspen Dynamics layout.

Table S1 summarizes the responses of CS1 and clearly reveals a strong asymmetry. Under negative disturbances, the W_{comp} decreases roughly in proportion to the reduced Q_{reb}. In contrast, under positive disturbances the W_{comp} rises disproportionately. This behavior is not primarily caused by the required Q_{reb} itself. For example, for the + 20% throughput case, the Q_{reb} increases by about 20%, consistent with the increase in overhead vapor flow V_t. However, the FVC flow rate V_r increases from 7.31 to 42.38 kmol/h, approximately 6 times. As a result, the total vapor flow through the compressors V_{hp} increases much more than the throughput (+ 44.06%), which drives both a large increase in Q_{trim} and a disproportionate rise in W_{comp}. The same pattern is observed for the + 20% MeOH disturbance, where V_r again increases dramatically. Therefore, the asymmetry of CS1 should be attributed to a disproportionate amplification of V_r under positive disturbances: the control structure allows the closed FVC loop to respond by boosting V_r rather than adjusting duties and pressures in an energy-efficient manner. This mechanism increases W_{comp} well beyond what is needed to meet the additional Q_{reb}, which motivates the revised pressure and energy coordination introduced in CS3 – CS6.

To explore which constraints in CS1 drive the asymmetric responses, we start with the degree of freedom analysis. The number of CDOF equals the number of manipulated variables (MVs). In practice, this number corresponds to the adjustable valves plus other adjustable electrical and mechanical variables (Skogestad, 2004). Therefore, in addition to the 3 compressor shaft works, 7 CDOFs (Fig. 3**a**) are provided by control valves, corresponding to the valves V1, V2, V3, V4, V6, V8, and the condenser outlet valve (not explicitly shown) in Fig. 3**b**. Valves V5 and V7 are included only to satisfy Aspen Dynamics requirements and are specified with negligible pressure drop; they therefore have no control effect and are not treated as CDOFs.

The resulting pairings between MVs and CVs for CS1 are as follows:

- The temperature of the sensitive stage is controlled by manipulating the compressor power; this pairing is needed to ensure single-end control of the distillation column.
- CDOF 1 (V1) acts as throughput manipulator and CDOF 3 (V3) sets the reflux ratio; these assignments are appropriate.
- Level control is implemented using CDOFs 4, 5, and 6 (V4, V6, and V8); this is required for inventory control.
- Column top pressure control is implemented using CDOF 7 (COND) and compressor discharge pressure control is implemented using CDOF 2 (V2); this choice is modified in the following control structures (CS3 – CS6).

Following the approach of Luyben (Luyben, 2016), we implemented for CS1 and CS2 two pressure controllers where PC2 manipulates valve V2 (CDOF 2) to control the compressor discharge pressure (stream 8). The results show good control of the column top pressure by PC1. In contrast, the discharge pressure cannot be controlled satisfactorily. The nominal discharge pressure is 6.26 bar. Under – 20% throughput and composition disturbances, the discharge pressure remains well-controlled. However, under + 20% throughput and + 20% MeOH disturbances, valve V2 becomes fully open and the discharge pressure rises to 6.53 and 6.40 bar, respectively. These results suggest that keeping the compressor discharge pressure constant is not a good self-optimizing CV, as it leads to poor performance and drives valve V2 to saturation.

The behavior of valve V2 can be interpreted using the Aspen Dynamics simple valve model, in which the valve flow satisfies:

$$F = C_0\sqrt{\frac{\rho_m \Delta P_{act}}{2M_w}} \tag{9}$$

With:

$$C_0 = \frac{Pos}{100}C_0^{\max} \tag{10}$$

Here, $F[kmol \bullet h^{-1}]$ is the molar flow rate through the valve, M_w $[kg \bullet kmol^{-1}]$ is the molecular weight, C_0 $[m^{1.5} \bullet kg^{0.5} \bullet h^{-1} \bullet bar^{-0.5}]$ is flow coefficient, $C_0^{\max}$ is maximum flow coefficient ($C_0^{\max} = 205.445$ in valve V2), Pos is the valve opening position (default at 50%), ρ_m $[kmol \bullet m^{-3}]$ is the molar density at the valve inlet, and ΔP_{act} $[bar]$ is the actual pressure drop across the valve. This relation shows that the achievable flow change depends on both the valve opening and the actual valve pressure drop. At nominal conditions, V2 operates at 50% opening and therefore retains sufficient adjustment range. Under positive disturbances, however, V2 becomes saturated rapidly. Additional numerical tests under gradually increasing throughput disturbances show that, for the base valve sizing, V2 remains below saturation up to about + 13% throughput, but reaches 100% opening at about + 14% throughput and stays saturated thereafter. These results are summarized in Table S2, which also shows that the valve pressure drop changes only modestly, whereas the flow increase is eventually limited by the valve-opening bound. In this sense, V2 saturation reduces the effective authority of the discharge pressure loop and introduces a marked nonlinearity: before saturation, the loop gain depends on both valve position and pressure drop (Eq. 9), whereas after saturation it depends only on the remaining pressure drop variation. Additional tests with much larger $C_0^{\max}$ valves showed that simply increasing the maximum flow coefficient does not remove this limitation. Even when $C_0^{MAX}$was increased substantially, the coupled series pressure loop caused the column pressure to become poorly regulated and V2 still approached saturation rapidly. This indicates that the observed infeasibility of constant compressor discharge pressure control is not merely a valve-sizing issue, but a structural limitation of the pressure control policy in the present strict series FVC loop.

Let us explain why holding the compressor discharge pressure constant is a poor choice for the FVC process, even though it works well in Luyben's MVR system (Luyben, 2016). In Luyben's flowsheets (Figs. 4, 5, and 8), a pre-compressor splitter creates two pressure paths (a compressed branch and an uncompressed bypass branch). This parallel pressure path provides an additional independent pressure degree of freedom, so the discharge pressure can be held at a fixed setpoint to achieve effective control. By contrast, the FVC process has no such parallel loop: the overhead vapor, compressor, condenser, and reflux drum form a strict series loop. In such a series loop there is essentially only one independent pressure degree of freedom: once the column top pressure is controlled, forcing the compressor discharge pressure to remain constant strongly restricts how the heat pump loop can respond to disturbances.

The drastic surge in V_r under positive disturbances can be explained by the combined heat transfer and flashing behavior of the condenser/reflux drum section. In the present Aspen Dynamics implementation, both the overall heat transfer coefficient U and the heat transfer area A are fixed. Therefore, the reboiler-side heat transfer is governed by changes in the temperature driving force $LMTD$ ($Q_{reb} = UA \bullet LMTD$). Under positive disturbances, the process requires more useful heat to be delivered through the heat pump loop. However, when the compressor discharge pressure is constrained, the available increase in $LMTD$ is limited. As a result, the condenser outlet condition is pushed toward saturation instead of remaining comfortably subcooled.

This effect is directly reflected in Table 2. In CS1, the condenser degree of subcooling decreases from 39.3 °C at nominal conditions to only 0.3 °C under the + 20% throughput disturbance and to 0.4 °C under the + 20% MeOH disturbance. Once the liquid leaving the condenser becomes only weakly subcooled, the subsequent pressure reduction causes much stronger flashing. This flashing generates a large recycle vapor flow V_r, which explains why the positive disturbances produce such a drastic surge in internal circulation.

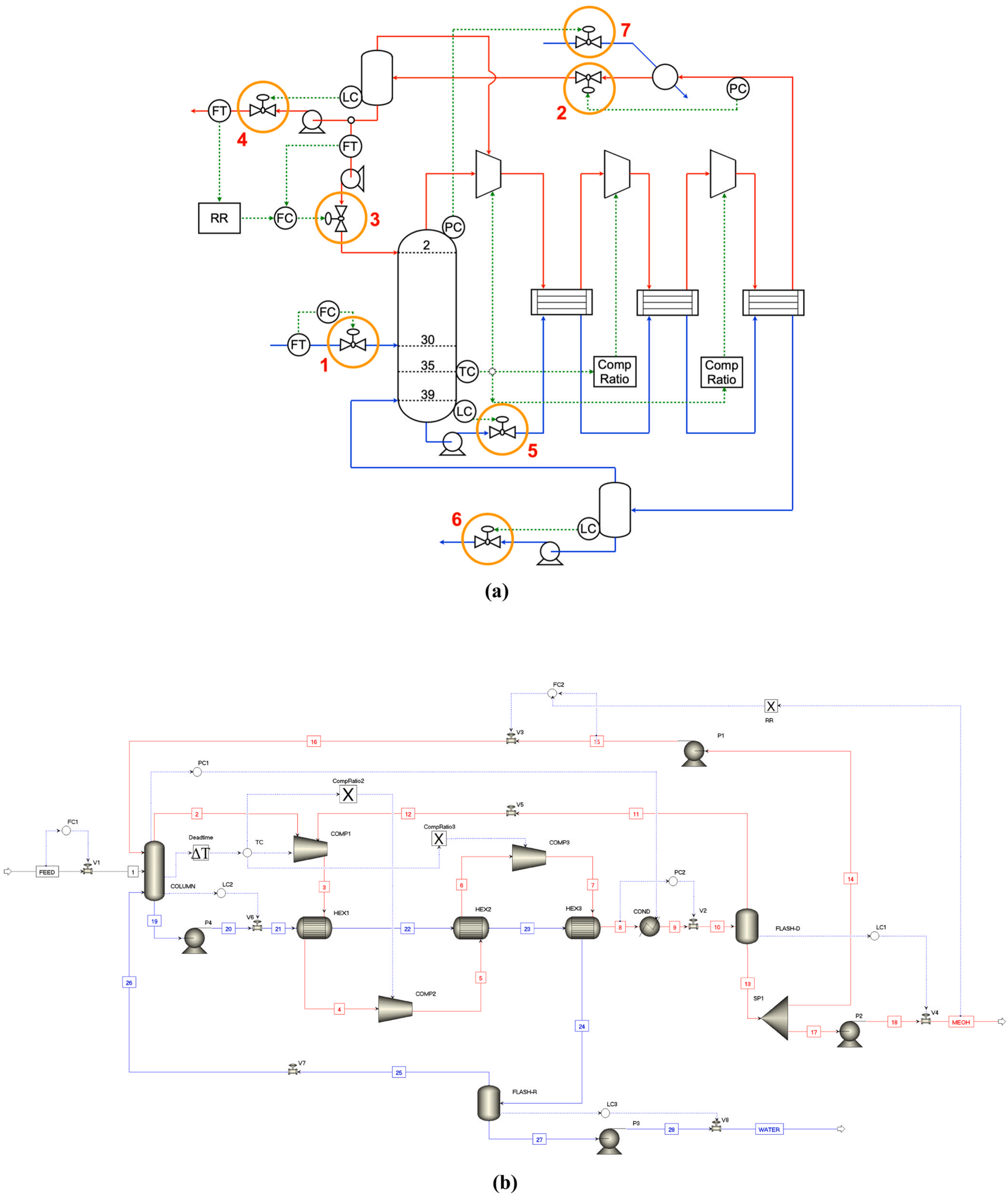

Fig. 3. CS1 control structure and Aspen Dynamics implementation. (a) Schematic control structure of CS1, where the sensitive-stage temperature is controlled by compressor power, the reflux ratio is fixed, the column top pressure is controlled by the condenser outlet valve, and the compressor discharge pressure is controlled by valve V2. Level controllers are used for inventory control. (b) Aspen Dynamics layout used for the dynamic simulations.

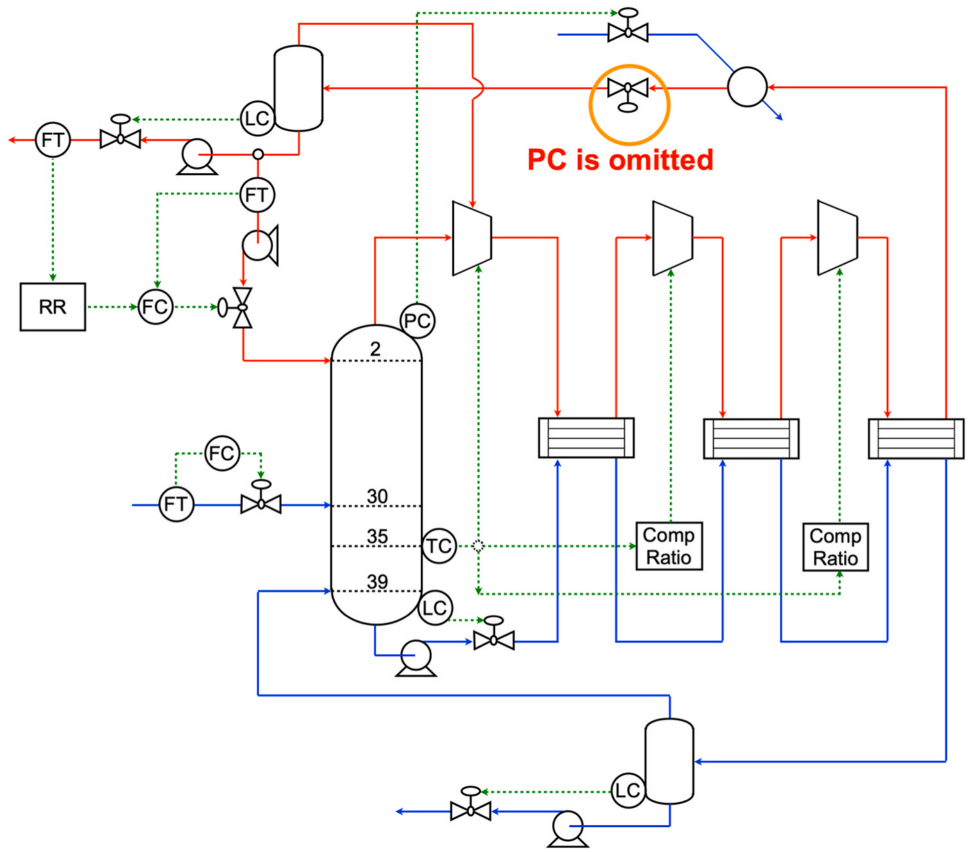

Fig. 4. CS3 control structure obtained by removing the compressor discharge pressure controller from CS1. Valve V2 is kept at a fixed opening of 50%, while the column top pressure, sensitive-stage temperature, and liquid levels are controlled by the same regulatory loops as in CS1. Green dashed lines denote control signals.

The resulting rise in V_r has a direct energy consequence. A larger recycle flow means that more latent heat is carried around the FVC loop. Since not all of this energy can be utilized as useful Q_{reb}, the excess heat must be rejected in the trim condenser. Therefore, Q_{trim} increases strongly when V_r surges. According to Eq. (7), this directly increases the compressor power W_{comp}. In other words, the poor energy performance of CS1 and CS2 under positive disturbances originates from the fact that the fixed compressor discharge pressure pushes the condenser outlet toward saturation, intensifies flashing after depressurization, and thereby creates an unnecessarily large recycle loop.

This interpretation also explains the logic of the subsequent control development. CS3 removes the fixed compressor discharge pressure constraint and thereby suppresses the excessive recycle amplification caused by strong flashing under positive disturbances. CS4 and CS5 then use the released degree of freedom more explicitly by controlling condenser outlet conditions, so that the flashing tendency can be regulated directly. This forms the basis for the more balanced and energy-efficient behavior observed in the later control structures.

4. Intermediate control structures CS3

Removing PC2 for compressor discharge pressure releases the additional CDOF associated with valve V2. In the intermediate control structure CS3 (Fig. 4), valve V2 is held at a fixed opening of 50%, which is effectively equivalent to tight valve position control. In the subsequent control structures (CS4 – CS6), this released CDOF is used explicitly, as discussed in the next section. The purpose of CS3 is thus not to provide the final control solution, but to isolate the effect of removing the compressor discharge pressure constraint and to examine whether this already improves the closed-loop behavior of the series FVC loop.

The CS3 is subjected to ± 20% step changes in throughput (Fig. 5) and ± 20% step changes in feed MeOH composition (Fig. 6), introduced at 0.5 h and completed after 10 h. Compared to CS1, CS3 exhibits markedly more symmetric responses and a lower compressor power penalty. The key reason is that the compressor discharge pressure is no longer forced to remain at a fixed setpoint. Instead, the system can respond through a more natural coordination between pressure lift and vapor circulation, which restores flexibility to the heat pump loop.

Under throughput disturbances, the benefit of removing PC2 is particularly clear (see Table 2 and Table 4). For + 20% throughput change, the compressor discharge pressure is allowed to rise, which increases the temperature driving force in the condenser/reboiler heat exchange loop. As a result, the additional reboiler duty can be supplied without the excessive recycle amplification observed in CS1. For − 20% throughput change, the discharge pressure is allowed to decrease, and the corresponding reduction in pressure lift is compensated by a moderate increase in recycle flow V_r. In this way, CS3 avoids the strongly asymmetric behavior seen in CS1, where the fixed discharge pressure choice forces the system to respond mainly through large changes in internal circulation. Overall, the throughput responses of CS3 show that the required heat duty can be delivered through different combinations of pressure lift and circulating vapor flow, and that releasing the discharge pressure constraint allows the process to choose a more favorable balance between the two variables.

A similar mechanism is observed under feed composition disturbances. When + 20% MeOH disturbance is introduced, the separation requires additional reboiler duty. In CS3, this demand is accommodated mainly by a higher discharge pressure, rather than by a disproportionate increase in recycle flow. When − 20% MeOH disturbance is introduced, the compressor discharge pressure is allowed to fall, and the recycle flow increases only to the extent needed to compensate for the lower pressure lift. This again produces a more balanced response than in CS1. The

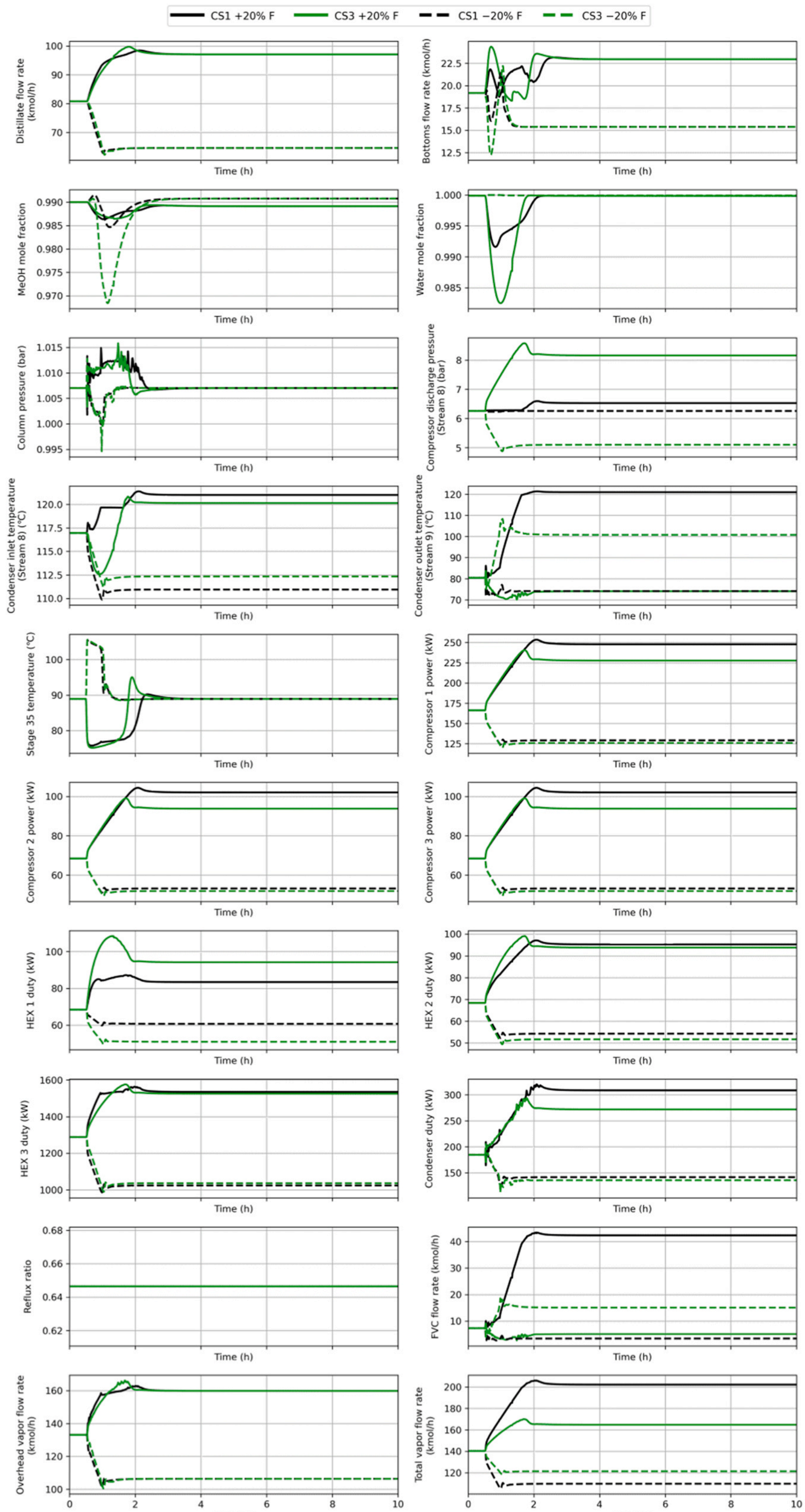

Fig. 5. Dynamic responses of CS1/CS3 under ± 20% throughput disturbance.

Table 2
Relationship among key control variables under disturbances.

Control structure	Nominal	+ 20% F	− 20% F	+ 20% MeOH	− 20% MeOH
CS1					
Compressor discharge pressure (bar)	6.26	6.53	6.26	6.40	6.26
FVC flow rate (kmol/h)	7.31	42.38	3.41	41.39	7.27
Condenser inlet temperature (°C)	117.0	121.0	110.9	120.2	111.7
Condenser outlet temperature (°C)	80.5	121.0	74.2	120.2	84.0
MeOH saturation temperature (°C)*	119.8	121.3	119.8	120.6	119.8
Degree of subcooling (°C)**	39.3	0.3	45.6	0.4	35.8
CS3					
Compressor discharge pressure (bar)	6.26	8.16	5.10	7.77	5.20
FVC flow rate (kmol/h)	7.31	5.08	15.08	2.06	15.73
Condenser inlet temperature (°C)	117.0	120.1	112.3	119.9	113.2
Condenser outlet temperature (°C)	80.5	74.1	100.8	68.5	102.0
MeOH saturation temperature (°C)*	119.8	129.5	112.6	127.7	113.3
Degree of subcooling (°C)**	39.3	55.4	11.8	59.2	11.3
CS4					
Compressor discharge pressure (bar)	6.26	7.19	5.43	6.66	6.81
FVC flow rate (kmol/h)	7.31	8.77	5.85	8.79	5.83
Condenser inlet temperature (°C)	117.0	121.7	112.2	121.6	111.0
Condenser outlet temperature (°C)	80.5	80.5	80.5	80.5	80.5
MeOH saturation temperature (°C)*	119.8	124.8	114.8	122.0	122.8
Degree of subcooling (°C)**	39.3	44.3	34.3	41.5	42.3
CS5					
Compressor discharge pressure (bar)	6.26	6.79	5.78	6.65	6.55
FVC flow rate (kmol/h)	7.31	10.56	4.74	10.11	6.49
Condenser inlet temperature (°C)	117.0	122.4	111.6	121.5	111.3
Condenser outlet temperature (°C)	80.5	83.4	77.7	82.7	82.1
MeOH saturation temperature (°C)*	119.8	122.7	117.0	122.0	121.4
Degree of subcooling (°C)**	39.3	39.3	39.3	39.3	39.3

* MeOH saturation temperature is calculated based on the compressor discharge pressure and Eq. (12)

** Degree of subcooling is calculated via Eq. (11), the difference of MeOH saturation temperature and condenser outlet temperature

overall effect is that CS3 reduces the energetic penalty associated with large internal circulation and improves the symmetry of the closed-loop responses for both positive and negative composition disturbances.

These results confirm the central point of the previous section: in the present FVC configuration, fixing the compressor discharge pressure is not a suitable SOC policy because it removes an important degree of freedom from an already strict series pressure loop. By contrast, simply holding valve V2 at a fixed opening already provides a more reasonable SOC choice. Although CS3 is not yet the final control structure, it clearly demonstrates that removing the redundant discharge pressure constraint restores a more favorable trade-off between pressure lift and circulating vapor flow, leading to more symmetric responses and lower compressor-power demand. This observation motivates the search, in the next section, for still better self-optimizing CVs that use the released degree of freedom more explicitly.

5. Selection of CVs for better SOC

CS1 and CS2 confirm that holding the compressor discharge pressure constant is a poor self-optimizing CV. CS3 shows that keeping valve V2 at a fixed position can serve as a reasonably good SOC choice. To further minimize W_{comp}, a better CV is still desired. In CS3, removing PC2 leaves valve V2 as an available CDOF, which may be used as a MV. Eq. (7) suggests that the remaining CDOF can be used to minimize Q_{trim} and therefore lower W_{comp}. Therefore, two candidate CVs are considered. One is the condenser outlet temperature (CS4) and the other is the degree of subcooling ΔT_{sub} in the condenser (CS5). These choices are partially inspired by Jensen and Skogestad (Jensen and Skogestad, 2007a, 2007b), who studied SOC of a stand-alone vapor recompression cycle. Interestingly, they also found that constant valve position (CS3) is a better self-optimizing CV than constant discharge compressor pressure (CS1 and CS2).

Starting from CS3, we initially assigned valve V2 to control the condenser outlet temperature (stream 9) and used condenser duty to control the column top pressure. As shown in Fig. S1, this configuration did not perform well dynamically because adjusting valve V2 has only a limited effect on the condenser outlet temperature. We therefore revise the pairings. Valve V2 is used to control the column top pressure, and condenser duty is used to control the proposed two controlled temperature variables.

5.1. Control structure CS4

As shown in Fig. 7, CS4 allows deliberate adjustment of the Q_{trim}, and hence of the W_{comp}.

Under throughput disturbance (Fig. 8), CS4 exhibits a much more symmetric response than both CS1 and CS3. Because the condenser outlet temperature is held constant, the recycle flow V_r and the heat pump circulation V_{hp} adjust in a much more proportional way to the imposed throughput change. This avoids the strong amplification of recycle observed in CS1 and also removes the inverse trend seen in CS3, where positive and negative throughput changes drive the recycle flow in opposite directions. In other words, CS4 allows the process to maintain a more balanced coordination between discharge pressure, flashing behavior, and vapor circulation, which lead to a more regular closed-loop response. The detailed steady-state values are listed in Table 2, but the main observation is that CS4 makes the internal flows scale much more naturally with the disturbance magnitude.

The same improvement is observed for feed composition disturbances (Fig. 9). When the feed MeOH composition changes, CS4 maintains the condenser outlet state directly and thereby prevents the condenser behavior from drifting toward either excessive flashing or excessive subcooling. As a result, the recycle flow remains within a moderate range and the system can accommodate the changing reboiler duty demand without the extreme circulation changes seen in CS1. Compared to CS3, the response is also more regular, because the selected temperature variable directly reflects the condenser outlet condition rather than only holding the valve at a fixed position. This makes CS4 a more physically interpretable SOC structure.

Overall, the results indicate that condenser outlet temperature is a good self-optimizing CV for the present FVC system. Compared with constant compressor discharge pressure control of CS1, CS4 suppresses the undesirable recycle amplification and provides a more symmetric and energetically favorable response. It also improves upon the more indirect constant valve position choice of CS3 by directly regulating a

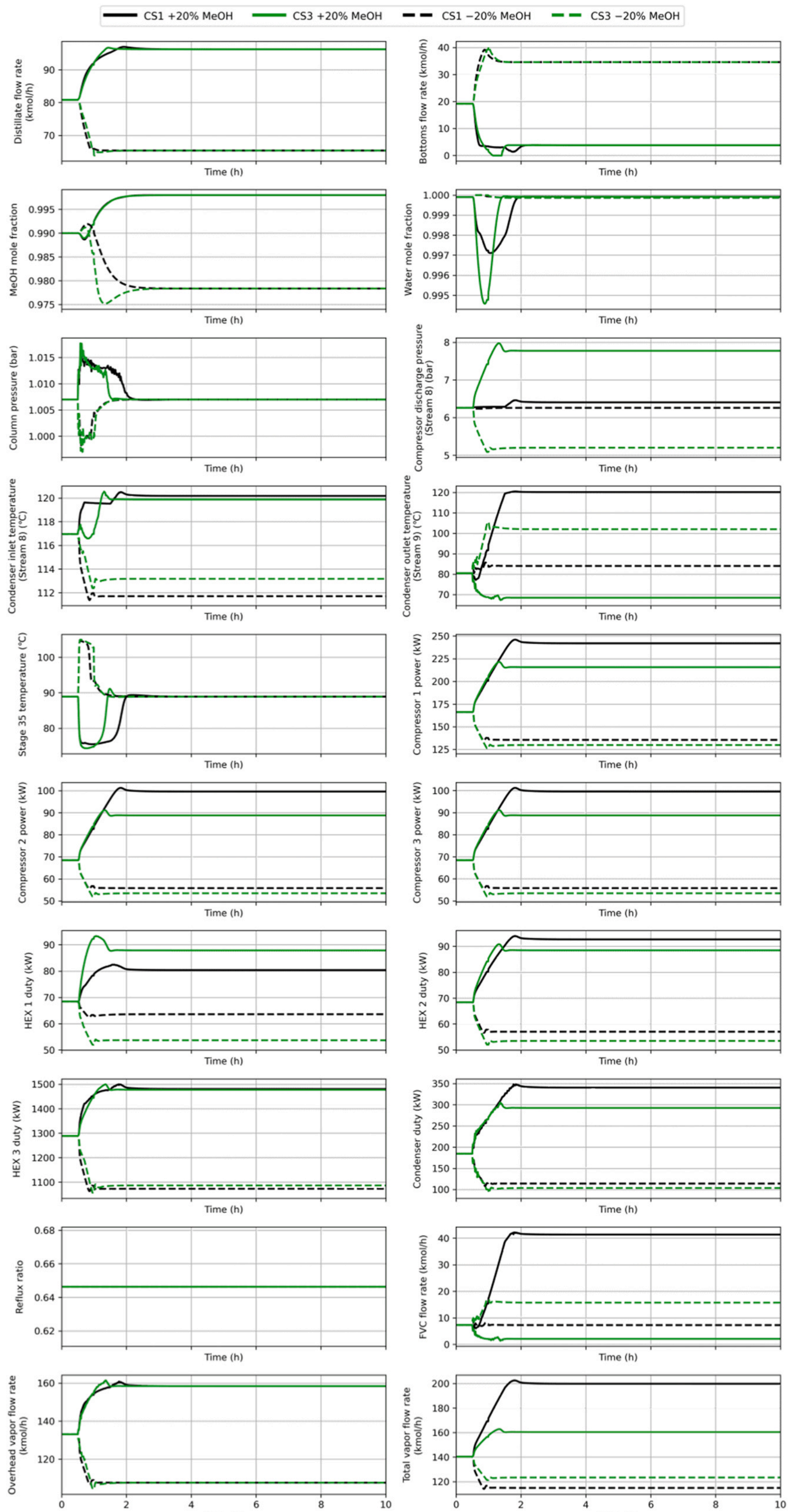

Fig. 6. Dynamic responses of CS1/CS3 under ± 20% MeOH composition disturbance.

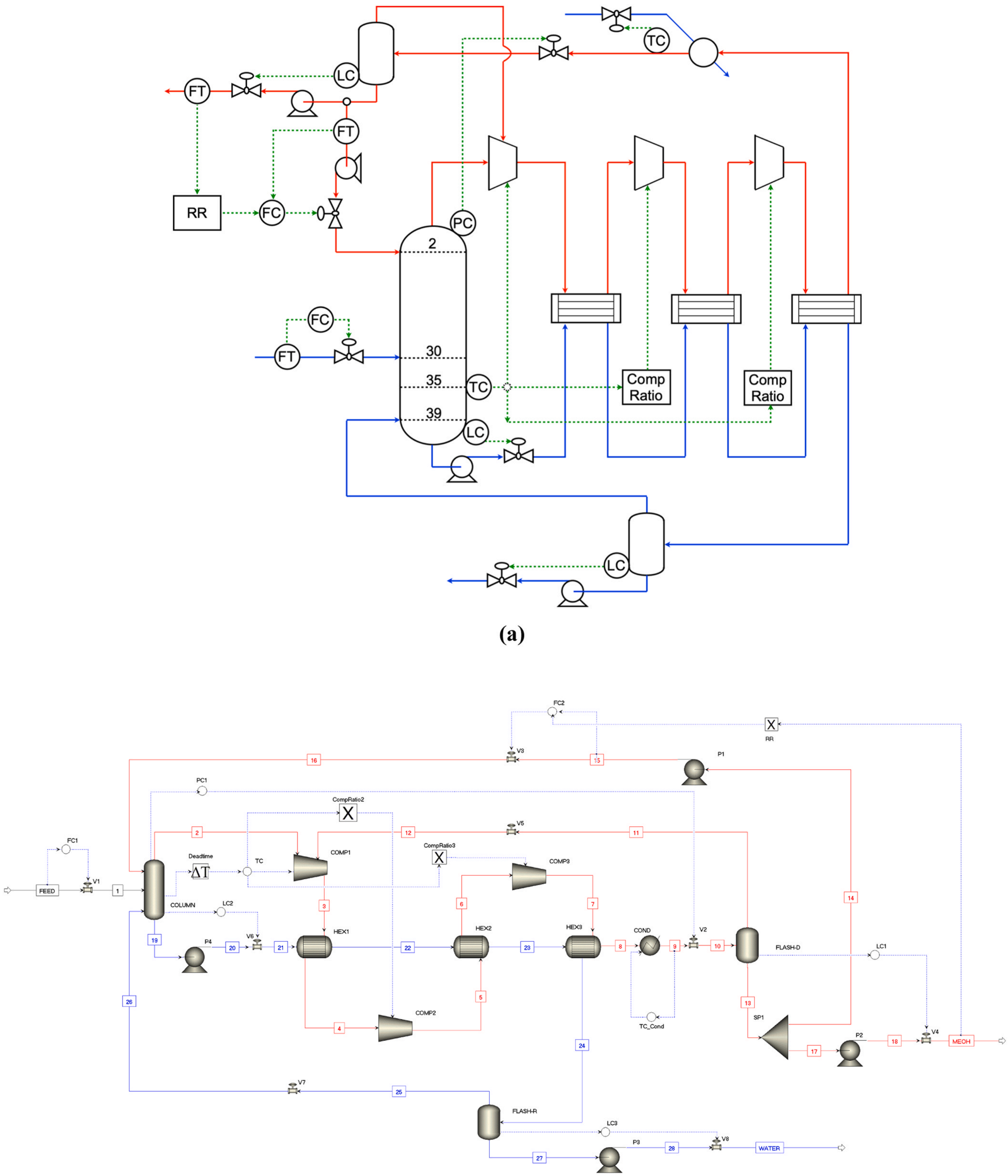

Fig. 7. CS4/CS5 control structure and Aspen Dynamics implementation. (a) Schematic control structure where valve V2 controls the column top pressure and the condenser duty controls the condenser outlet condition. In CS4, the condenser outlet temperature is held constant; in CS5, the condenser degree of subcooling is held constant using a pressure-dependent saturation-temperature calculation. The sensitive-stage temperature and liquid levels are controlled by the same regulatory loops as in CS3. (b) Aspen Dynamics layout used for the dynamic simulations.

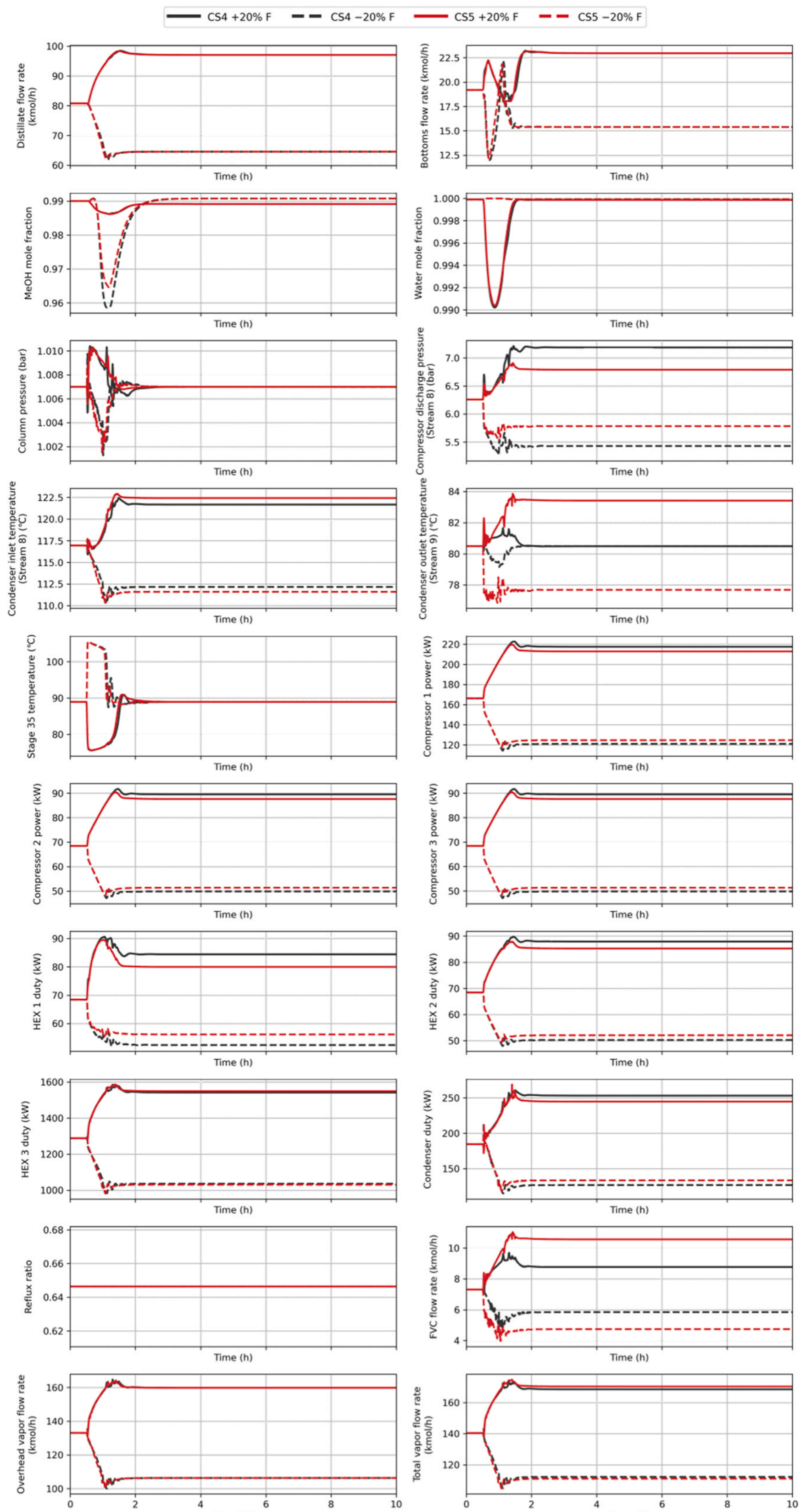

Fig. 8. Dynamic responses of CS4/CS5 under ± 20% throughput disturbance.

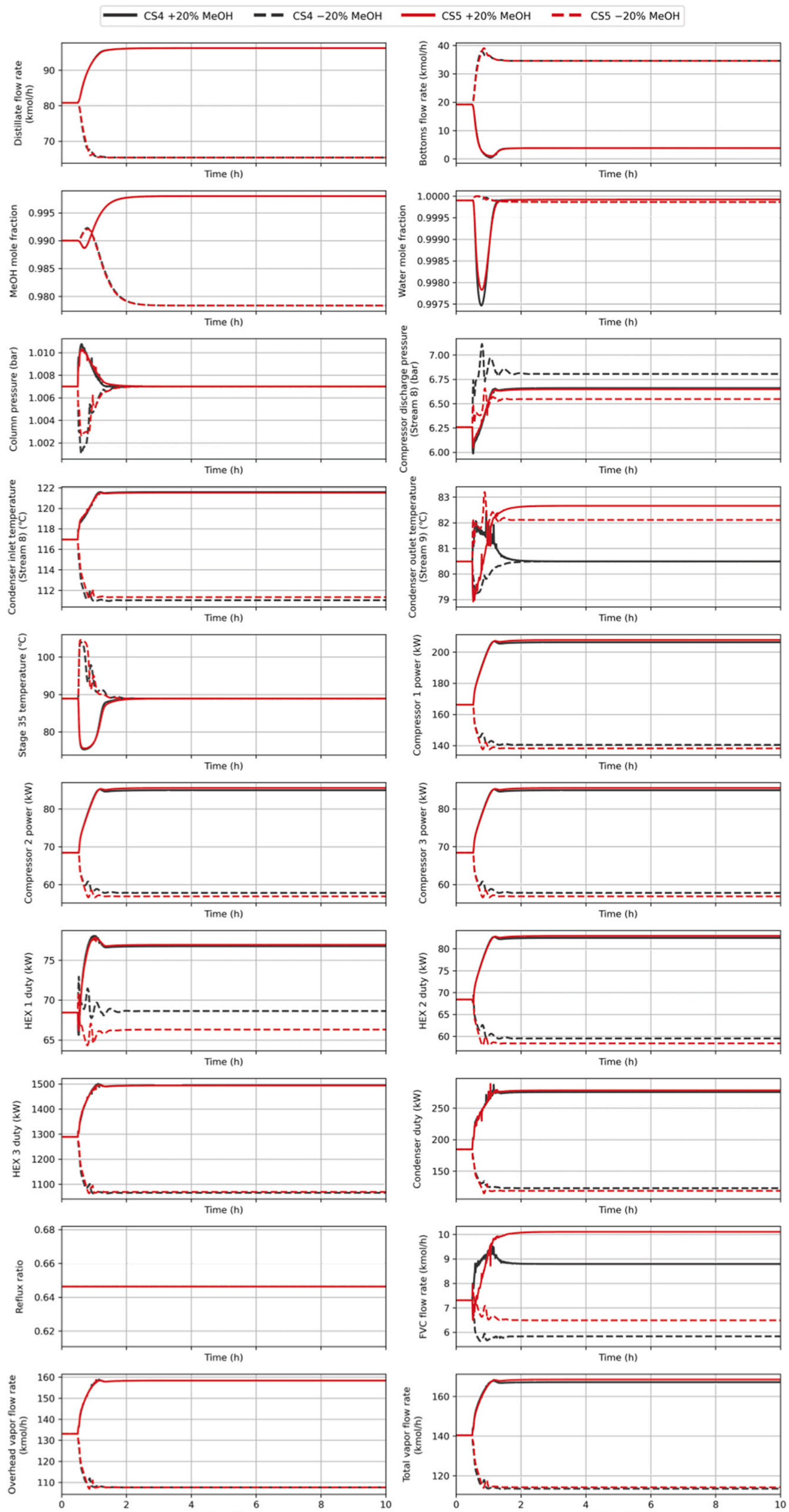

Fig. 9. Dynamic responses of CS4/CS5 under ± 20% MeOH composition disturbance.

physically meaningful condenser outlet condition. Although it does not minimize compressor power in every individual case, CS4 offers a well-balanced trade-off among energy performance, recycle moderation, and response regularity, which is consistent with the objective of SOC. This supports the idea that condenser outlet conditions provide a better basis for SOC than compressor discharge pressure in a strict series FVC loop. The next section examines whether the condenser degree of subcooling can provide similar or further improved performance.

5.2. Control structure CS5

This section evaluates whether the condenser degree of subcooling can serve as a good self-optimizing CV. When the condenser outlet is close to saturation, flashing is significant and the V_r can increase sharply. When the outlet is more subcooled, flashing is reduced and the V_r tends to be smaller. This trend can be viewed in Table 2. In CS1 the degree of subcooling collapses to almost zero under positive disturbances so the V_r becomes very large. In CS3 the degree of subcooling becomes large under positive disturbances and the V_r becomes small. Under negative disturbances the opposite happens. In CS4 the condenser outlet temperature is tightly controlled so the degree of subcooling stays closer to its nominal value and the V_r remains within a narrower band.

Comments. In Table 2, the condenser degree of subcooling ΔT_{sub} is calculated by the difference of MeOH saturation temperature $T_{sat,MeOH}$ and condenser outlet temperature $T_{cond,out}$:

$$\Delta T_{sub} = T_{sat,MeOH}\left(P_{cond,in}\right) - T_{cond,out} \tag{11}$$

The MeOH saturation temperature is calculated via Antoine correlation:

$$\log_{10}(P) = A - \frac{B}{T + C} \tag{12}$$

Where P is the saturation pressure in [bar] and T is the saturation temperature in [K]. This work adopts the high temperature parameter set reported by NIST for MeOH, which is valid over 353–483 K (Hirata et al., 1967). The constants are $A = 5.31301$, $B = 1676.569$, and $C = -21.728$.

The control structures of CS4 and CS5 are the same. The only difference is the setpoint definition. In CS4 the setpoint of the condenser outlet temperature “TC_Cond” (Fig. 7**b**) is held at 80.5 °C, whereas in CS5 the setpoint is constant degree of subcooling of 39.3 °C. This setpoint is implemented in Aspen Dynamics using a flowsheet equation that updates the required condenser outlet temperature based on the current compressor discharge pressure (condenser inlet pressure), as shown in Fig. 10.

Under both throughput and feed composition disturbances, CS5 gives dynamic responses that are very similar to those of CS4. The main qualitative difference is that CS5 keeps the subcooling from drifting toward either very low values or excessively high values. Because of this constraint, the recycle flow and discharge pressure adjust in a coordinated way, and the resulting responses remain regular and well-behaved over the tested disturbance range. In practical terms, CS5 provides the same general benefit as CS4: it avoids the undesirable recycle amplification associated with constant compressor discharge pressure control and maintains much more balanced operation than CS1.

Overall, CS5 further supports the use of condenser-outlet-based variables as practical SOC choices for the present FVC system. By explicitly regulating the condenser degree of subcooling, CS5 avoids the unfavorable behavior associated with fixing the compressor discharge pressure and provides energy performance broadly comparable to that of CS4. Although it is not uniformly superior in every disturbed case, it confirms the key design principle emerging from this study, namely that condenser outlet conditions are much better CV candidates for SOC than compressor discharge pressure in a strict series FVC loop. Compared to CS4, however, CS5 is somewhat more involved in implementation because it requires an additional pressure measurement and a pressure-dependent saturation-temperature calculation. For this reason, although CS5 is a valid and physically attractive alternative, CS4 remains the simpler choice for further development. The next section therefore uses CS4 as the basis for adding explicit composition control in order to enforce the product specification.

5.3. Control structure CS6

Although CS4 and CS5 improve dynamic behavior and exhibit comparable electric power consumption, neither structure includes a CC. As a result, they cannot enforce the product composition target explicitly. For example, under a + 20% MeOH disturbance the distillate becomes over-purified to 0.998, whereas under a – 20% MeOH disturbance it stabilizes at about 0.978. Such deviations either waste energy through unnecessary separation or result in off-spec product. To prevent both over- and under-purification, a CC is introduced in CS6 (Fig. 11). Compared to CS4, CS5 requires an additional pressure measurement and an auxiliary calculation, which increase implementation complexity. For this reason, CS4 is selected as the basis for CS6. In this way, CS6 aims to retain the favorable dynamic and energetic features of CS4 while tightening product quality control and reducing avoidable energy use associated with over-purity.

It should be noted that, in the SOC framework, CS6 operates on two distinct time scales. Ideally, SOC assumes that a constant setpoint for the selected CV gives an acceptable economic loss at steady-state. However, when a perfectly ideal self-optimizing CV does not exist across all operating conditions, its setpoint needs to be updated on a slower time scale. In CS6, the faster inner self-optimizing controller (condenser outlet temperature at fixed setpoint) has the key role of manipulating the input to provide close-to-optimal operation (maintaining an acceptable

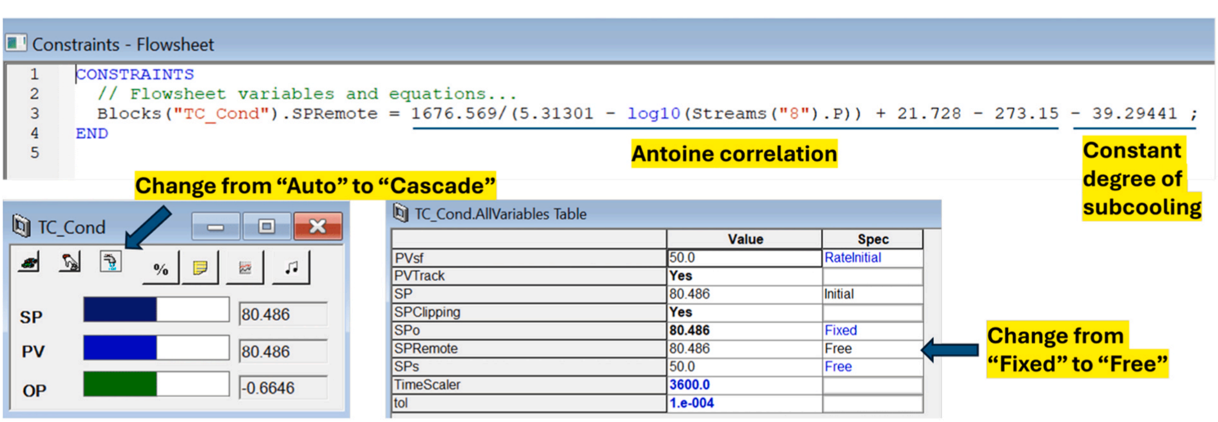

Fig. 10. Aspen Dynamics setting for constant degree of subcooling in CS5.

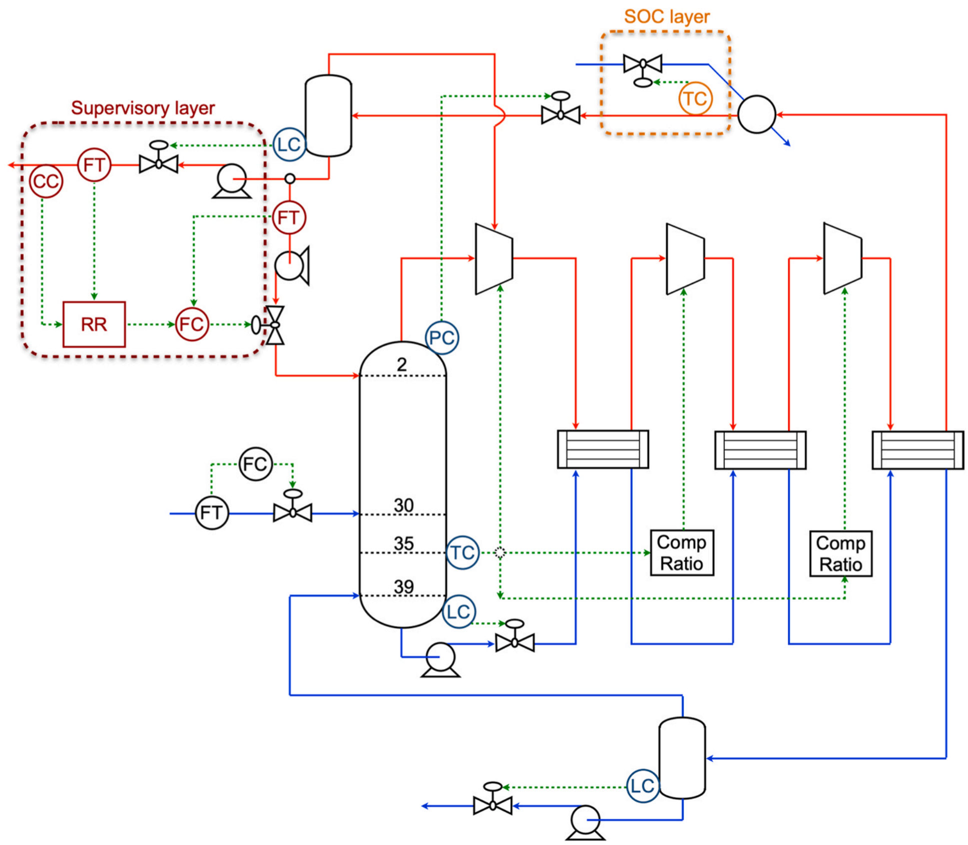

Fig. 11. Control structure CS6. Green dashed lines denote control signals. Inner regulatory loops (temperature, pressure, level) are shown in navy blue; the SOC layer (condenser outlet temperature) in amber orange; the supervisory layer (composition controller) in burgundy red.

economic loss) within the time period between each setpoint update. Meanwhile, the outer composition controller acts as the supervisory layer that updates the separation effort setpoint on a slower time scale to strictly enforce the product specification (Skogestad, 2023).

In CS6, the distillate water impurity measured in the distillate product stream is controlled by manipulating the reflux ratio. A measurement deadtime of 3 min is included to represent analyzer delay. The composition controller is implemented as a PI controller, and its parameters are obtained using the Tyreus–Luyben tuning rule. The composition loop is intentionally designed to be slower than the fast regulatory loops, through conservative PI tuning and the inclusion of longer analyzer deadtime, in order to avoid unnecessary interaction with the underlying temperature- and pressure-related control structure. No explicit anti-windup scheme is included for this controller in the present simulations. The column-top pressure and condenser outlet temperature control loops remain the same as in CS4, so that the added composition loop acts as a supervisory quality-control layer rather than replacing the existing SOC structure.

Under throughput disturbance (Fig. 12), CS6 largely preserves the favorable closed-loop behavior of CS4. The responses remain symmetric and well-behaved, and the additional CC loop only slightly adjusts the reflux ratio to keep the distillate composition close to its target. As a result, the overall behavior under throughput changes is very similar to that of CS4: the process remains near an energetically efficient operating region, while product purity is regulated more tightly. This shows that adding CC does not fundamentally disturb the advantageous SOC behavior already achieved in CS4.

The main benefit of CS6 becomes more apparent under MeOH composition disturbances (Fig. 13). In these cases, the additional CC adjusts the reflux ratio in a more targeted way, so that the distillate composition is kept close to its specification. Compared to CS4, this results in a more appropriate use of separation effort, because the process no longer consumes extra energy to produce unnecessarily high purity, nor does it allow the distillate purity to fall below the target. In this sense, CS6 improves the practical usefulness of the control system by combining good energy performance with explicit product specifications.

The price for this improvement is a somewhat slower transient response. Because the added CC is tuned more slowly than the regulatory loops, the approach to the new steady-state becomes less rapid, particularly for disturbances that directly affect the distillate composition. This trade-off is expected: tighter CC improves steady-state product quality and avoids energy waste, but it also introduces slower dynamics. Even so, the overall response of CS6 remains well-behaved and industrially more relevant than that of the purely single-end SOC structures when strict product specifications must be satisfied.

Overall, CS6 shows that the condenser outlet temperature policy of CS4 can be used as an effective self-optimizing CV, while an additional CC provides the regulatory action needed to enforce the distillate specification. Relative to CS4, the key advantage of CS6 is therefore not a universal reduction in compressor power under every disturbance, but a better balance between energy efficiency and guaranteed product quality. This makes CS6 a practical structure when the process must operate close to an energetically efficient regime without sacrificing product purity.

5.4. Validation of self-optimizing CVs

The previous comparisons are based on single-end control structures. As a result, the achieved product purities may deviate slightly from the specified targets, especially under feed composition disturbances. Because the economic objective is the compressor power W_{comp}, a fair comparison of candidate self-optimizing CVs should be made at identical product specifications. In this section, the proposed self-optimizing CVs

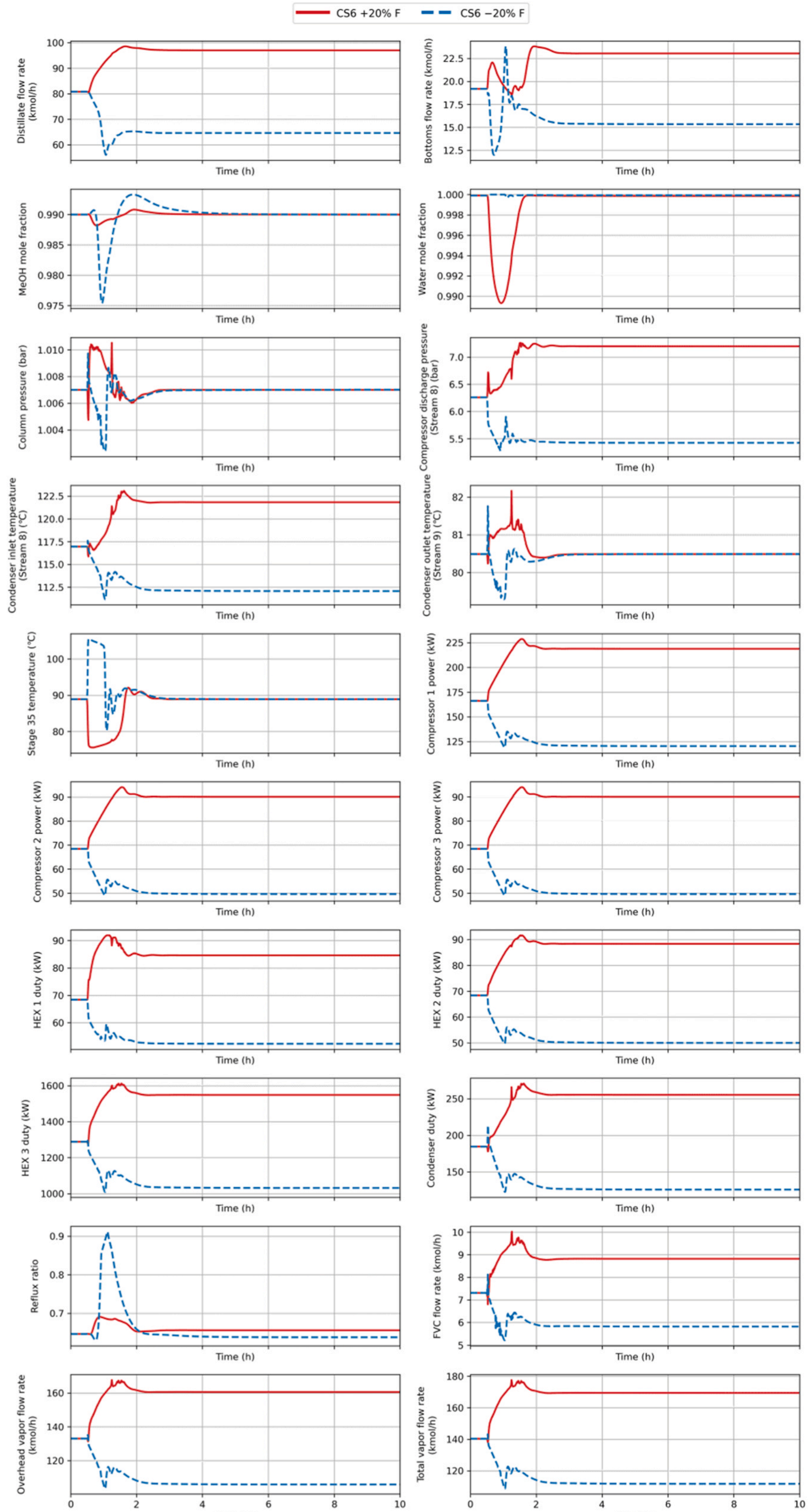

Fig. 12. Dynamic responses of CS6 under ± 20% throughput disturbance.

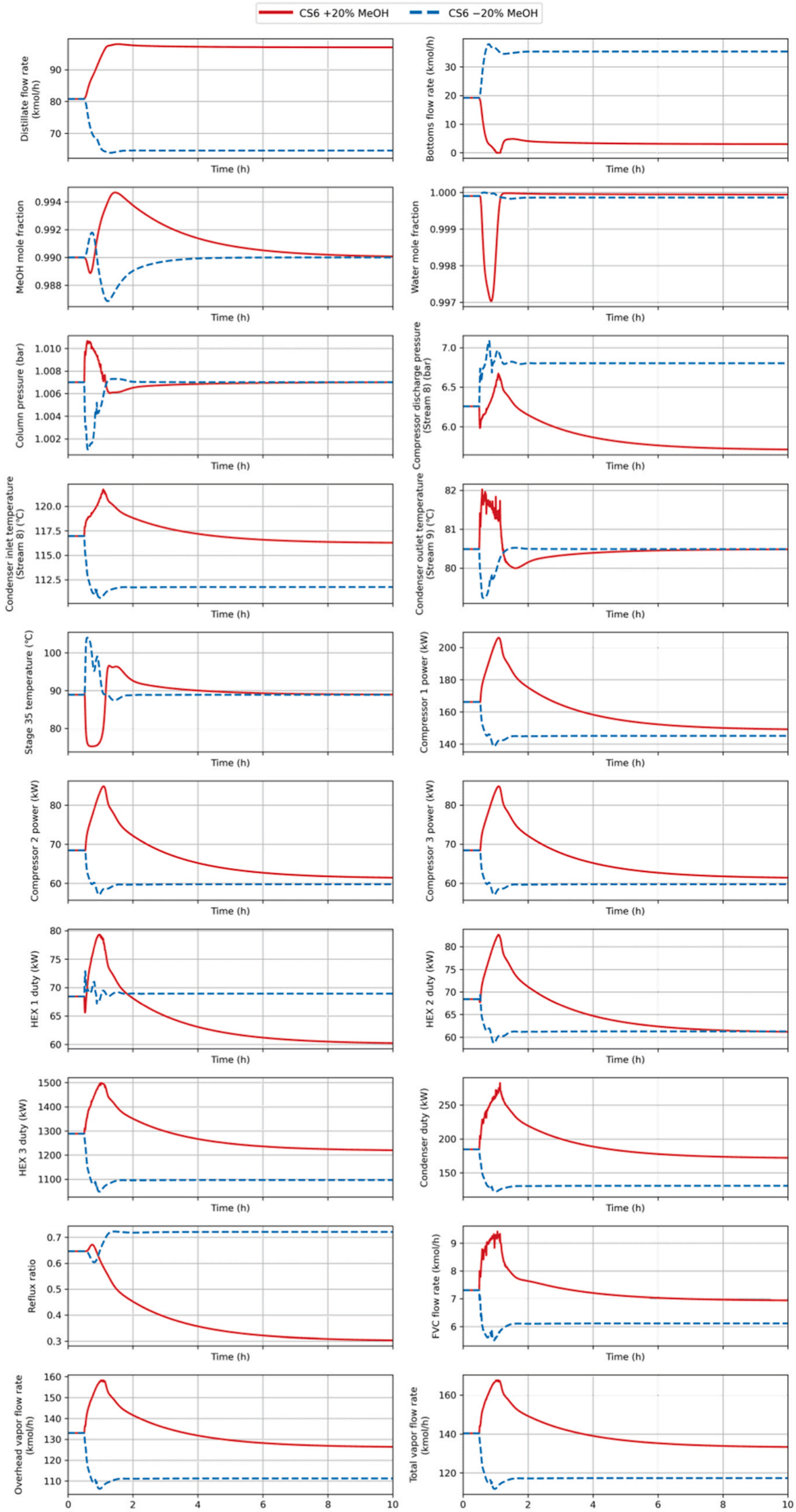

Fig. 13. Dynamic responses of CS6 under ± 20% MeOH composition disturbance.

are therefore validated using steady-state results obtained under the same distillate and bottoms purities, without emphasizing transient performance.

To enforce identical product specifications, the original single-end control structures are modified to dual-end composition control in all cases. The distillate MeOH purity is controlled by a CC manipulating the reflux ratio, while the bottoms water purity is maintained by adjusting the compressor power through a composition/temperature cascade control loop. The composition loops are tuned sufficiently slowly to ensure convergence, and steady-state values are recorded after the responses have fully settled. This setup allows a consistent assessment of how different self-optimizing CVs affect W_{comp} when the separation task is fixed.

Four candidate self-optimizing CVs are evaluated: (i) constant compressor discharge pressure, (ii) constant valve V2 opening, (iii) constant condenser outlet temperature (80.5 °C), and (iv) constant condenser degree of subcooling (39.3 °C). The resulting steady-state performance is summarized in Table 3. As expected, for a given disturbance, the Q_{reb} is essentially the same for all four cases because the feed conditions and the product specifications are identical. Differences in energy performance therefore primarily reflect differences in W_{comp} and Q_{trim}.

Table 3
Validation of the self-optimizing CVs.

Self-optimizing CV	Nominal	+ 20% F	− 20% F	+ 20% MeOH	− 20% MeOH
Constant compressor discharge pressure					
MeOH composition	0.99	0.99	0.99	0.99	0.99
Water composition	0.9999	0.9999	0.9999	0.9999	0.9999
Compressor power (kW)	303 (0%)	456 (+ 50.38%)	234 (− 22.66%)	280 (− 7.55%)	256 (− 15.68%)
Reboiler duty (kW)	1425 (0%)	1722 (+ 20.77%)	1134 (− 20.46%)	1330 (− 6.72%)	1227 (− 13.92%)
Condenser duty (kW)	185 (0%)	312 (+ 69.08%)	141 (− 23.85%)	180 (− 2.39%)	122 (− 34.10%)
COP	4.70 (0%)	3.78 (− 19.69%)	4.84 (+ 2.85%)	4.75 (+ 0.90%)	4.80 (+ 2.08%)
Constant valve V2 opening					
MeOH composition	0.99	0.99	0.99	0.99	0.99
Water composition	0.9999	0.9999	0.9999	0.9999	0.9999
Compressor power (kW)	303 (0%)	419 (+ 38.19%)	229 (− 24.54%)	269 (− 11.32%)	244 (− 19.49%)
Reboiler duty (kW)	1425 (0%)	1722 (+ 20.77%)	1134 (− 20.46%)	1330 (− 6.72%)	1227 (− 13.92%)
Condenser duty (kW)	185 (0%)	275 (+ 49.06%)	135 (− 26.94%)	169 (− 8.57%)	110 (− 40.37%)
COP	4.70 (0%)	4.11 (− 12.60%)	4.96 (+ 5.41%)	4.95 (+ 5.18%)	5.03 (+ 6.92%)
Constant condenser outlet temperature					
MeOH composition	0.99	0.99	0.99	0.99	0.99
Water composition	0.9999	0.9999	0.9999	0.9999	0.9999
Compressor power (kW)	303 (0%)	399 (+ 31.70%)	220 (− 27.55%)	269 (− 11.28%)	265 (− 12.64%)
Reboiler duty (kW)	1425 (0%)	1722 (+ 20.77%)	1134 (− 20.46%)	1330 (− 6.72%)	1227 (− 13.92%)
Condenser duty (kW)	185 (0%)	256 (+ 38.41%)	126 (− 31.87%)	169 (− 8.52%)	131 (− 29.11%)
COP	4.70 (0%)	4.31 (− 8.30%)	5.16 (+ 9.79%)	4.95 (+ 5.15%)	4.63 (− 1.47%)
Constant condenser degree of subcooling					
MeOH composition	0.99	0.99	0.99	0.99	0.99
Water composition	0.9999	0.9999	0.9999	0.9999	0.9999
Compressor power (kW)	303 (0%)	391 (+ 29.12%)	226 (− 25.36%)	274 (− 9.66%)	261 (− 14.03%)
Reboiler duty (kW)	1425 (0%)	1722 (+ 20.77%)	1134 (− 20.46%)	1330 (− 6.72%)	1227 (− 13.92%)
Condenser duty (kW)	185 (0%)	248 (+ 34.18%)	132 (− 28.28%)	174 (− 5.85%)	127 (− 31.39%)
COP	4.70 (0%)	4.40 (− 6.47%)	5.01 (+ 6.57%)	4.86 (+3.27%)	4.71 (+ 0.12%)

Table 3 indicates that constant compressor discharge pressure is generally the least attractive SOC choice. It gives the highest compressor power performance in most of the disturbed cases and remains inferior to the alternative choices when the separation task is fixed. This confirms that fixing the compressor discharge pressure is a poor SOC choice for the present FVC system. Among the remaining three candidates, the relative ranking depends on the disturbance type. For throughput disturbances, the condenser-outlet-based variables perform best: constant condenser degree of subcooling gives the most favorable result for + 20% throughput case, while constant condenser outlet temperature performs best for the − 20% throughput disturbance. For feed composition disturbances, constant valve V2 opening becomes more competitive: it gives the most favorable result for both + 20% MeOH and − 20% MeOH disturbances.

Overall, the results confirm that near-optimal operation can be achieved without fixing the compressor discharge pressure. Constant V2 opening, constant condenser outlet temperature, and constant condenser degree of subcooling all provide substantially better SOC behavior than constant discharge pressure, although their relative ranking is disturbance dependent. This also suggests that no single self-optimizing CV is uniformly superior over the entire operating region. From a practical viewpoint, constant condenser outlet temperature remains an attractive choice because it delivers consistently competitive performance while avoiding the pressure-dependent saturation calculation required for subcooling control and the limited transferability associated with fixing a specific valve opening.

To explicitly quantify SOC performance, an economic loss metric (L) is introduced to compare the candidate variables against a re-optimized benchmark:

$$L = \frac{W_{comp,CS} - W_{comp,opt}}{W_{comp,opt}} \times 100\% \quad (13)$$

As shown in Table 4, the benchmark value ($W_{comp,opt}$) is established as the minimum compressor power obtained among the tested candidate CV policies under dual-composition control for each disturbance scenario in Table 3. This benchmark is used to quantify the economic loss within the investigated operating scenarios, rather than to represent a global dynamic economic optimum over the entire feasible operating region. The economic loss (L) for the proposed self-optimizing CVs, namely condenser outlet temperature (used in CS4 and CS6) and condenser degree of subcooling (used in CS5), relative to this re-

Table 4
Economic loss analysis of candidate self-optimizing CVs.

Metric	Nominal	+ 20% F	− 20% F	+ 20% MeOH	− 20% MeOH
$W_{comp,opt}$ (kW)	303	391	220	269	244
Economic loss L*					
Constant compressor discharge pressure (used in CS1 & CS2)	0%	16.46%	6.74%	4.25%	4.74%
Constant valve V2 opening (used in CS3)	0%	7.02%	4.15%	0%	0%
Constant condenser outlet temperature (used in CS4 & CS6)	0%	2.00%	0%	0.04%	8.52%
Constant condenser degree of subcooling (used in CS5)	0%	0%	3.02%	1.87%	6.79%

* This evaluation is based on the steady-state "energy-at-spec" data to ensure a fair thermodynamic comparison.

optimized benchmark is below 8.52% and 6.79%, respectively, across all tested disturbances. In contrast, the original constant compressor discharge pressure policy (used in CS1 and CS2) yields losses up to 16.46%, while the constant valve opening (used in CS3) shows intermediate losses up to 7.02%. These results quantitatively confirm that the condenser-outlet-based structures maintain an acceptably low economic loss without the need for real-time setpoint re-optimization, which is perfectly consistent with the SOC criterion.

To further illustrate the sensitivity of the condenser-outlet-based SOC structure to heat exchanger sizing, an additional sensitivity test was performed by varying the *UA* values of the three heat exchangers (HEX1, HEX2, and HEX3) simultaneously by ± 20%. The tests were conducted using the dual-end composition control structure based on CS4 to enforce identical product specifications, with the condenser outlet temperature setpoint was kept at 80.5 °C. When − 20% *UA* is introduced, a larger *LMTD* is required to deliver the same reboiler duty of 1425 kW. Consequently, the compressor discharge pressure dynamically rises from the nominal 6.26 bar to 6.96 bar. This increases the required total compressor power W_{comp} from 303.0 kW to 323.8 kW, while the trim condenser duty Q_{trim} increases proportionally from 184.6 kW to 205.4 kW. Conversely, when + 20% *UA* is introduced, the compressor discharge pressure drops to 5.81 bar, reducing W_{comp} to 289.0 kW and Q_{trim} to 170.6 kW. Within this UA variation test, the proposed SOC structure accommodates the heat-transfer-capacity changes without requiring structural modification or setpoint re-tuning.

Furthermore, it is important to note that the constant difference between compressor power and trim condenser duty across these varying *UA* scenarios perfectly validates the proxy relationship in Eq. 7. By calculating Φ as the difference $W_{comp} - Q_{trim}$, we obtain exactly 118.4 kW for all three tested scenarios: the nominal case (303.0 − 184.6 = 118.4 kW), the − 20% *UA* case (323.8 − 205.4 = 118.4 kW), and the + 20% *UA* case (289.0 − 170.6 = 118.4 kW). This invariant result perfectly matches the nominal Φ value previously established in Table 1. It should be emphasized, however, that this sensitivity test is limited to simultaneous *UA* variations. The compressor isentropic efficiency and the minimum allowable temperature approach are kept fixed at their nominal assumptions, namely 0.75 and 10 °C, respectively (Cui et al., 2024b). Sensitivity to these additional design assumptions is outside the scope of the present dynamic comparison and is left for future work. Overall, the sensitivity analysis demonstrates that minimizing Q_{trim} is a robust proxy for minimizing W_{comp}, regardless of non-idealities in heat exchanger sizing or changing temperature approaches.

5.5. Generalizable design workflow

To systematically address the control challenges of fully electrified heat pump assisted distillation systems, a three-step transferable design workflow is proposed. This methodology generalizes the findings of the present study beyond the specific methanol/water case, providing a structured approach for designing SOC systems in similar FVC processes:

(1) Series-loop degree of freedom test: Check whether fixing the compressor discharge pressure over-constrains the series pressure drop. If both the column top pressure and the compressor discharge pressure are controlled simultaneously, the system lacks the flexibility to balance pressure lift and vapor circulation. In such cases, one pressure loop must be released to restore the necessary degree of freedom.

(2) Economic proxy selection: Use the energy balance equation $W_{comp} = Q_{trim} + \Phi$ (Eq. 7) to identify the trim condenser duty (Q_{trim}) as the key quantity to minimize. Screen candidate CVs (such as valve position, condenser outlet temperature, or condenser outlet degree of subcooling) for their ability to indirectly reflect or tightly bound Q_{trim} under disturbances.

(3) Validation under product specifications: Apply dual-end composition control (as demonstrated in **Section 5.4**) to validate the screened candidate variables. This step compares the required compressor power (W_{comp}) at fixed product specifications across different self-optimizing CVs and disturbance scenarios.

6. Control performance

This section evaluates the control performance of the proposed control structures from three complementary perspectives: overall energy consumption, dynamic response speed as measured by settling time, and tracking accuracy quantified by integrated absolute error (IAE). Together, these indicators allow a systematic comparison of how each self-optimizing CV affects both the economic efficiency and the tightness of product quality control under throughput and composition disturbances.

It should be noted that the dynamic comparisons in this section are mainly presented on an "energy-at-achieved-purity" basis. In particular, CS1, CS3, CS4, and CS5 are temperature-based structures intended to represent practical scenarios where composition analyzers may be avoided, while CS2 and CS6 include an additional distillate composition controller mainly to illustrate the effect of adding composition control. A standardized "energy-at-spec" comparison can be viewed in Table 3.

Table 5 gives a summary of the energy performance. Overall, CS1/CS2 shows the largest increase in W_{comp} and the largest deterioration in COP, thus confirming that the compressor discharge pressure is a poor self-optimizing CV. CS3 performs better because the removal of the redundant pressure control loop, which reduces W_{comp} and improves COP. CS4/CS5 further controls condenser outlet temperature, leading to more symmetric and energy-efficient responses. It should be mentioned that for control structures without CC, it might be too optimistic for the corresponding COP because the methanol product purity is not rigorously satisfied. Finally, CS6 adds CC on top of CS4, tightening product purity without a significant penalty in energy consumption, so that it combines tight product quality control with high energy efficiency.

Table S3 compares the settling times of the MeOH and water compositions. The settling time is defined as the time for the controlled product composition process variable (PV) to enter and remain within a ± 1% of its specification value (e.g., 0.9801–0.9999 mol fraction for $x_D = 0.99$). CS1 and CS3 exhibit relatively short and similar settling times, typically around 1.8–2.5 h for MeOH and ≤ 1.6 h for water. CS4 and CS5 further reduce or at least maintain these settling times, giving the fastest overall response among the control structures. In contrast, the configurations with explicit composition controllers (CS2 and CS6) show noticeably slower MeOH dynamics, especially for + 20% MeOH disturbances, where the settling time increases to about 9.5 h. Water composition, however, remains comparatively fast and similar across all structures. These results confirm that adding CC improves steady-state purity and energy efficiency, but at the expense of longer transients, whereas CS4 and CS5 offer a good compromise between response speed and economic performance. It should be emphasized that the disturbance tests reported in this work are step changes. No systematic ramp-disturbance simulations are included. Since a ± 20% step change imposes a more abrupt load on the control system than a ramp change of the same magnitude, the present step tests are expected to provide a conservative indication of closed-loop robustness. Nevertheless, the detailed evaluation of ramp disturbances, including different ramp rates and electricity-following operation, is left for future work.

Table S4 compares the IAEs of MeOH and water compositions. The IAE is calculated using the built-in Aspen Dynamics IAE block. The error signal is the absolute deviation of the controlled composition from its specification (0.99 for MeOH and 0.9999 for water), expressed in mole fraction units. Thus, the reported IAE corresponds to:

$$IAE = \int_0^T |e(t)|dt \tag{14}$$

Table 5
Comparison of energy consumption*.

Control structure	Nominal	+ 20% F	− 20% F	+ 20% MeOH	− 20% MeOH
CS1					
MeOH composition	0.99	0.989122	0.990759	0.997992	0.978358
Water composition	0.9999	0.999863	0.999924	0.999918	0.999862
Compressor power (kW)	303 (0%)	452 (+ 49.13%)	235 (− 22.30%)	441 (+ 45.55%)	247 (− 18.47%)
Reboiler duty (kW)	1425 (0%)	1714 (+ 20.22%)	1138 (− 20.14%)	1654 (+ 16.01%)	1194 (− 16.24%)
Condenser duty (kW)	185 (0%)	308 (+ 67.08%)	142 (− 23.28%)	340 (+ 84.39%)	114 (− 38.24%)
COP	4.70 (0%)	3.79 (− 19.38%)	4.83 (+ 2.78%)	3.75 (− 20.29%)	4.83 (+ 2.73%)
CS2					
MeOH composition	0.99	0.99	0.99	0.99	0.99
Water composition	0.9999	0.999861	0.999925	0.999940	0.999858
Compressor power (kW)	303 (0%)	455 (+ 50.29%)	234 (− 22.64%)	283 (− 6.60%)	255 (− 15.70%)
Reboiler duty (kW)	1425 (0%)	1721 (+ 20.75%)	1134 (− 20.45%)	1342 (− 5.88%)	1227 (− 13.93%)
Condenser duty (kW)	185 (0%)	312 (+ 68.92%)	141 (− 23.82%)	183 (− 0.83%)	122 (− 34.13%)
COP	4.70 (0%)	3.78 (− 19.65%)	4.84 (+ 2.84%)	4.74 (+ 0.77%)	4.80 (+ 2.10%)
CS3					
MeOH composition	0.99	0.989130	0.990755	0.997994	0.978359
Water composition	0.9999	0.999863	0.999925	0.999911	0.999862
Compressor power (kW)	303 (0%)	415 (+ 37.03%)	230 (− 24.21%)	393 (+ 29.74%)	237 (− 21.90%)
Reboiler duty (kW)	1425 (0%)	1714 (+ 20.22%)	1138 (− 20.14%)	1654 (+ 16.01%)	1194 (− 16.24%)
Condenser duty (kW)	185 (0%)	272 (+ 47.22%)	136 (− 26.42%)	292 (+ 58.43%)	104 (− 43.87%)
COP	4.70 (0%)	4.13 (− 12.27%)	4.96 (+ 5.37%)	4.21 (− 10.58%)	5.04 (+ 7.25%)
CS4					
MeOH composition	0.99	0.989129	0.990754	0.997992	0.978358
Water composition	0.9999	0.999863	0.999924	0.999921	0.999861
Compressor power (kW)	303 (0%)	396 (+ 30.83%)	221 (− 27.18%)	376 (+ 24.15%)	256 (− 15.52%)
Reboiler duty (kW)	1425 (0%)	1714 (+ 20.22%)	1138 (− 20.14%)	1654 (+ 16.01%)	1194 (− 16.24%)
Condenser duty (kW)	185 (0%)	253 (+ 37.04%)	127 (− 31.29%)	276 (+ 49.26%)	123 (− 33.39%)
COP	4.70 (0%)	4.32 (− 8.11%)	5.16 (+ 9.67%)	4.40 (− 6.55%)	4.66 (− 0.85%)
CS5					
MeOH composition	0.99	0.989128	0.990754	0.997994	0.978350
Water composition	0.9999	0.999863	0.999925	0.999918	0.999862
Compressor power (kW)	303 (0%)	388 (+ 28.06%)	227 (− 24.99%)	379 (+ 25.02%)	252 (− 16.88%)
Reboiler duty (kW)	1425 (0%)	1714 (+ 20.22%)	1138 (− 20.14%)	1654 (+ 16.01%)	1194 (− 16.24%)
Condenser duty (kW)	185 (0%)	245 (+ 32.49%)	133 (− 27.70%)	278 (+ 50.69%)	119 (− 35.62%)
COP	4.70 (0%)	4.42 (− 6.12%)	5.01 (+ 6.47%)	4.36 (− 7.21%)	4.74 (+ 0.77%)
CS6					
MeOH composition	0.99	0.99	0.99	0.99	0.99
Water composition	0.9999	0.999854	0.999924	0.999938	0.999858
Compressor power (kW)	303 (0%)	399 (+ 31.64%)	220 (− 27.52%)	272 (− 10.22%)	265 (− 12.68%)
Reboiler duty (kW)	1425 (0%)	1721 (+ 20.75%)	1134 (− 20.45%)	1342 (− 5.88%)	1227 (− 13.93%)
Condenser duty (kW)	185 (0%)	255 (+ 38.31%)	126 (− 31.83%)	172 (− 6.78%)	131 (− 29.17%)
COP	4.70 (0%)	4.31 (− 8.27%)	5.16 (+ 9.76%)	4.93 (+ 4.83%)	4.64 (− 1.44%)

* Values reported on an "energy-at-achieved-purity" basis; product compositions shown may deviate from specifications for CS1, CS3–CS5 (no CC). For "energy-at-spec" comparison, see Table 3.

where $e(t)$ is the mole fraction error and T is the evaluation time of 10 h for all cases. In the present study, the IAE values are not normalized by either the nominal value or the disturbance magnitude. The results show that structures with CC clearly outperform those without: IAE_{MeOH} and IAE_{Total} of CS2 and CS6 are one order of magnitude lower than others, particularly for MeOH disturbances. In all configurations the IAE for water remains very small, indicating that the bottoms specification is intrinsically easier to control than the distillate composition.

Overall, the study highlights SOC as a key principle for exploiting the FVC heat pump loop. The main limitation of CS1/CS2 is that fixing the compressor discharge pressure is a poor SOC choice because it over-constrains the series pressure loop and triggers asymmetric responses. By removing this redundant pressure constraint in CS3, the heat pump loop regains the CDOF to find a better balance between pressure lift and circulating vapor flow, which restores symmetry while maintaining comparable product regulation. Building on this idea, CS4 and CS5 deliberately select condenser outlet conditions as self-optimizing CVs: CS4 keeps a constant condenser outlet temperature, whereas CS5 keeps a constant degree of subcooling. Both deliver similar energy performance under the tested disturbances. Finally, CS6 adds a CC on top of CS4 to enforce product specifications. This eliminates both under and over purification and improves composition regulation, with somewhat longer transients due to the slower composition loop.

7. Conclusions

This work evaluates the dynamic operability of a fully electrified FVC-assisted distillation system and compares six alternative control structures. The results show that using constant compressor discharge pressure as a CV in CS1 and CS2 is a poor SOC choice. It produces strongly asymmetric responses and also degrades COP under disturbances. Removing this redundant pressure control in CS3 restores the available CDOF and improves response symmetry. Building on this, CS4 and CS5 adopt more appropriate self-optimizing CVs on condenser outlet conditions, reducing the compressor power. Finally, CS6 adds a CC to enforce the MeOH specification. It avoids both under-purification and over-purification, with only longer settling times caused by the slower composition loop. Overall, CS4, CS5, and CS6 offer a practical balance between energy efficiency and product quality control, and they are promising candidates for industrial implementation of FVC-assisted distillation.

Furthermore, a three-step design workflow is formulated, comprising a series-loop degree of freedom test, economic proxy selection, and validation of self-optimizing CVs under strictly enforced product specifications. This procedure offers a transferable methodology for developing low-loss SOC structures in heat pump assisted distillation systems and is not limited to the present methanol/water case study. The results demonstrated in this work are limited to the unconstrained FVC operating regime, where compressor saturation, dynamic electricity pricing, and grid-following power limitations are not explicitly imposed. For industrial applications under such constraints, a backup trim reboiler operated via split-range control is a promising future extension, but its dynamic evaluation is outside the scope of the present study.

CRediT authorship contribution statement

Anton A. Kiss: Writing – review & editing, Writing – original draft, Validation, Supervision, Methodology, Formal analysis, Data curation, Conceptualization. **Sigurd Skogestad:** Writing – review & editing, Writing – original draft, Validation, Methodology, Formal analysis, Conceptualization. **Xiaodong Zhang:** Writing – review & editing, Writing – original draft, Validation, Methodology, Formal analysis, Conceptualization. **Chengtian Cui:** Writing – review & editing, Writing – original draft, Visualization, Validation, Software, Methodology, Investigation, Formal analysis, Data curation, Conceptualization. **Meng Qi:** Writing – review & editing, Writing – original draft, Validation, Methodology, Formal analysis, Conceptualization.

Declaration of Competing Interest

The authors declare the following financial interests/personal relationships which may be considered as potential competing interests: Anton A. Kiss is member of the Editorial Board of Chemical Engineering Research and Design (ChERD).

Acknowledgments

This work was supported by the European Union HORIZON-MSCA-2024-PF-01 (No. 101211557).

Appendix A. Supporting information

Supplementary data associated with this article can be found in the online version at doi:10.1016/j.cherd.2026.05.017.

References

Adami, M., Farheen, K., Skiborowski, M., 2025a. Electrifying distillation – Optimization-based evaluation of internally heat-integrated distillation columns. Sep. Purif. Technol. 360, 131061. https://doi.org/10.1016/j.seppur.2024.131061.

Adami, M., Schnurr, J., Skiborowski, M., 2025b. Electrified distillation – Optimized design of closed cycle heat pumps with refrigerant selection and flash-enhanced mechanical vapor recompression. Appl. Therm. Eng. 273, 126559. https://doi.org/10.1016/j.applthermaleng.2025.126559.

Cui, C., Kiss, A.A., 2026. Process intensification of multi-stage heat pump assisted distillation with liquid injection. Chem. Eng. Process. Process. Intensif. 224, 110796. https://doi.org/10.1016/j.cep.2026.110796.

Cui, C., Li, Q., Luyben, W.L., Kiss, A.A., 2025a. Dynamics and control of discretely heat integrated distillation columns. Comput. Chem. Eng., 109144 https://doi.org/10.1016/j.compchemeng.2025.109144.

Cui, C., Liu, S., Sun, J., 2018. Optimal selection of operating pressure for distillation columns. Chem. Eng. Res. Des. 137. https://doi.org/10.1016/j.cherd.2018.07.028.

Cui, C., Qi, M., Zhang, X., Sun, J., Li, Q., Kiss, A.A., Wong, D.S.-H., Masuku, C.M., Lee, M., 2024a. Electrification of distillation for decarbonization: an overview and perspective. Renew. Sustain. Energy Rev. 199, 114522. https://doi.org/10.1016/j.rser.2024.114522.

Cui, C., van Reisen, J., Tyraskis, I., Kiss, A.A., 2025b. Efficient heat integration within discretely heat integrated distillation columns using liquid injection. AIChE J. https://doi.org/10.1002/aic.18861.

Cui, C., Zhang, Q., Zhang, X., Sun, J., Chien, I.-L., 2022. Dynamics and control of thermal- versus electrical-driven pressure-swing distillation to separate a minimum-boiling azeotrope. Sep. Purif. Technol. 280. https://doi.org/10.1016/j.seppur.2021.119839.

Cui, C., Zhang, X., Qi, M., Kiss, A.A., 2025c. Control of fully electrified heat pump assisted distillation process by flash vapor circulation. Chem. Eng. Res. Des. 220, 450–460. https://doi.org/10.1016/j.cherd.2025.07.023.

Cui, C., Zhang, X., Qi, M., Lyu, H., Sun, J., Kiss, A.A., 2024b. Fully electrified heat pump assisted distillation process by flash vapour circulation. Chem. Eng. Res. Des. 206, 280–284. https://doi.org/10.1016/j.cherd.2024.05.011.

Hirata, M., Suda, S., Onodera, Y., 1967. Vapor pressure of methanol in high pressure regions. Chem. Eng. 31, 339–342,a1. https://doi.org/10.1252/kakoronbunshu1953.31.339.

Jäschke, J., Cao, Y., Kariwala, V., 2017. Self-optimizing control – A survey. Annu. Rev. Control 43, 199–223. https://doi.org/10.1016/j.arcontrol.2017.03.001.

Jensen, J.B., Skogestad, S., 2007a. Optimal operation of simple refrigeration cycles: Part I: Degrees of freedom and optimality of sub-cooling. Comput. Chem. Eng. 31, 712–721. https://doi.org/10.1016/j.compchemeng.2006.12.003.

Jensen, J.B., Skogestad, S., 2007b. Optimal operation of simple refrigeration cycles: Part II: Selection of controlled variables. Comput. Chem. Eng. 31, 1590–1601. https://doi.org/10.1016/j.compchemeng.2007.01.008.

Jogwar, S.S., Daoutidis, P., 2009. Dynamics and control of vapor recompression distillation. J. Process Control 19, 1737–1750. https://doi.org/10.1016/j.jprocont.2009.07.001.

Karami, G., Amidpour, M., Sheibani, B.H., Salehi, G.R., 2015. Distillation column controllability analysis through heat pump integration. Chem. Eng. Process. Process. Intensif. 97, 23–37. https://doi.org/10.1016/j.cep.2015.08.005.

Khan, Md.M.N., Babu, G.U.B., Jana, A.K., 2012. Improving energy efficiency and cost-effectiveness of batch distillation for separating wide boiling constituents. 1. vapor recompression column. Ind. Eng. Chem. Res. 51, 15413–15422. https://doi.org/10.1021/ie300907b.

Kiss, A.A., Infante Ferreira, C.A., 2016. Heat Pumps in Chemical Process Industry. CRC Press. https://doi.org/10.1201/9781315371030.

Kiss, A.A., Smith, R., 2020. Rethinking energy use in distillation processes for a more sustainable chemical industry. Energy 203, 117788. https://doi.org/10.1016/j.energy.2020.117788.

Larsson, T., Hestetun, K., Hovland, E., Skogestad, S., 2001. Self-Optimizing Control of a Large-Scale Plant: The Tennessee Eastman Process. Ind. Eng. Chem. Res. 40, 4889–4901. https://doi.org/10.1021/ie000586y.

Luyben, W.L., 2026. Beware of gas compressor designs with sub-atmospheric suction pressures. Chem. Eng. Sci. 321, 122831. https://doi.org/10.1016/j.ces.2025.122831.

Luyben, W.L., 2018. Capital cost of compressors for conceptual design. Chem. Eng. Process. - Process. Intensif. 126, 206–209. https://doi.org/10.1016/j.cep.2018.01.020.

Luyben, W.L., 2016. Control of an azeotropic DWC with vapor recompression. Chem. Eng. Process. - Process. Intensif. 109, 114–124. https://doi.org/10.1016/j.cep.2016.08.013.

Patraşcu, I., Bîldea, C.S., Kiss, A.A., 2019. Dynamics and control of a heat pump assisted azeotropic dividing-wall column for biobutanol purification. Chem. Eng. Res. Des. 146, 416–426. https://doi.org/10.1016/j.cherd.2019.04.029.

Patraşcu, I., Bildea, C.S., Kiss, A.A., 2017. Dynamics and control of a heat pump assisted extractive dividing-wall column for bioethanol dehydration. Chem. Eng. Res. Des. 119, 66–74. https://doi.org/10.1016/j.cherd.2016.12.021.

Qi, M., Zhang, X., Wong, D.S., Shu, C., Cui, C., Kiss, A.A., 2025. Electrified distillation with flash vapor circulation and thermal storage for dynamic electricity markets. AIChE J. https://doi.org/10.1002/aic.18750.

Reyes-Lúa, A., 2020. Systematic design of advanced control structures. PhD Thesis. Norwegian University of Science and Technology (NTNU), Trondheim.

Skogestad, S., 2023. Advanced control using decomposition and simple elements. Annu. Rev. Control 56, 100903. https://doi.org/10.1016/j.arcontrol.2023.100903.

Skogestad, S., 2004. Control structure design for complete chemical plants. Comput. Chem. Eng. 28, 219–234. https://doi.org/10.1016/j.compchemeng.2003.08.002.

Skogestad, S., 2000. Plantwide control: the search for the self-optimizing control structure. J. Process Control 10, 487–507. https://doi.org/10.1016/S0959-1524(00)00023-8.

Yang, D., Wang, J., Ban, N., Zhong, Y., Wong, D.S.-H., Razminia, A., Cui, C., 2025a. Model predictive control of pressure-swing distillation via closed-loop system identification. J. Process Control 156, 103589. https://doi.org/10.1016/j.jprocont.2025.103589.

Yang, D., Wang, J., Cai, H., Rao, J., Cui, C., 2025b. Intelligent control strategy for electrified pressure-swing distillation processes using artificial neural networks-based composition controllers. Sep. Purif. Technol. 360, 130991. https://doi.org/10.1016/j.seppur.2024.130991.

Yang, D., Zhang, Q., Zhang, Q., Cui, C., 2023. Dynamics and control of electrified pressure-swing distillation for separating a maximum-boiling azeotrope featuring small pressure-induced shift. Sep. Purif. Technol. 312. https://doi.org/10.1016/j.seppur.2023.123360.

Zhang, X., Cui, C., Lyu, H., Sun, J., 2024. Integrated process design and self-optimizing control: a probabilistic approach. Chem. Eng. Sci. 286, 119667. https://doi.org/10.1016/j.ces.2023.119667.

Zhang, Xiaodong, Cui, C., Sun, J., Zhang, Xuemei, 2023. Integrated design and self-optimizing control of extractive distillation process with preconcentration. Chem. Eng. Sci. 280, 119074. https://doi.org/10.1016/j.ces.2023.119074.